Deducing mineralogy of serpentinized and carbonated ultramafic rocks using physical properties with implications for carbon sequestration and subduction zone dynamics

Jamie A Cutts[1], Katrin Steinthorsdottir[2], Connor C Turvey[2], Gregory Dipple[1], Randolph Jonathan Enkin[3], and Simon M Peacock[1]

[1]University of British Columbia
[2]The University of British Columbia
[3]Geological Survey of Canada

November 22, 2022

Abstract

Serpentinization of ultramafic rocks is fundamental to modern plate tectonics and for volatile (re-)cycling into the mantle and magmatic arcs. Serpentinites are also highly reactive with CO_2 such that they are prime targets for carbon sequestration. Serpentinization and carbonation of ultramafic rocks results in changes in their physical properties such that they should be detectable using geophysical surveys; this could provide constraint on the reactivity of rocks without extensive sample characterization. We constrain the physio-chemical relationships in altered ophiolitic ultramafic rocks using petrographic observations, major-element chemistry, quantitative X-ray diffraction, and physical properties on a suite of >400 samples from the Canadian Cordillera. Serpentinization results in a systematic decrease in density that reflects the increase in serpentine abundance and carbonation results in an increase in density, mostly reflecting the formation of magnesite; based on these data we present two formulations for determining extent of serpentinization: one based on major-element chemistry and the other on density. Magnetic susceptibility is variable during serpentinization; most harzburgitic samples show a 100-fold increase in magnetic susceptibility, whereas most dunitic samples and a minor proportion of harzburgitic samples show very little change in magnetic susceptibility. We use quantitative mineralogy and physical properties of the samples to constrain a model for using density and magnetic susceptibility to approximate the mineralogy of ultramafics rock. Although further work is required to understand the role of remanence in applying these models to geophysical data, this presents an advancement and opportunity to prospect for the most reactive ultramafic rocks for carbon sequestration.

Deducing mineralogy of serpentinized and carbonated ultramafic rocks using physical properties with implications for carbon sequestration and subduction zone dynamics

J. A. Cutts[1†], K. Steinthorsdottir[1], C. Turvey[1], G. M. Dipple[1], R. J. Enkin[2], and S. M. Peacock[1]

[1]CarbMin Lab, Department of Earth, Ocean and Atmospheric Sciences, The University of British Columbia, Vancouver, BC V6T 1Z4

[2]Geological Survey of Canada-Pacific, Sidney, British Columbia, Canada

[†]Corresponding author: Jamie Cutts (jcutts@eoas.ubc.ca)

Key Points:

- The density and magnetic susceptibility of ultramafic rocks change predictably during serpentinization (hydration) and carbonation
- Density is most effective at predicting the extent of alteration, whereas magnetic susceptibility may be subject to significant variability
- Physical properties can predict the mineralogy, alteration extent, and potential of ultramafic rocks for carbon sequestration

Abstract

Serpentinization of ultramafic rocks is fundamental to modern plate tectonics and for volatile (re-)cycling into the mantle and magmatic arcs. Serpentinites are also highly reactive with CO_2 such that they are prime targets for carbon sequestration. Serpentinization and carbonation of ultramafic rocks results in changes in their physical properties such that they should be detectable using geophysical surveys; this could provide constraint on the reactivity of rocks without extensive sample characterization. We constrain the physio-chemical relationships in altered ophiolitic ultramafic rocks using petrographic observations, major-element chemistry, quantitative X-ray diffraction, and physical properties on a suite of >400 samples from the Canadian Cordillera. Serpentinization results in a systematic decrease in density that reflects the increase in serpentine abundance and carbonation results in an increase in density, mostly reflecting the formation of magnesite; based on these data we present two formulations for determining extent of serpentinization: one based on major-element chemistry and the other on density. Magnetic susceptibility is variable during serpentinization; most harzburgitic samples show a 100-fold increase in magnetic susceptibility, whereas most dunitic samples and a minor proportion of harzburgitic samples show very little change in magnetic susceptibility. We use quantitative mineralogy and physical properties of the samples to constrain a model for using density and magnetic susceptibility to approximate the mineralogy of ultramafics rock. Although further work is required to understand the role of remanence in applying these models to geophysical data, this presents an advancement and opportunity to prospect for the most reactive ultramafic rocks for carbon sequestration.

Plain Language Summary

When mantle rocks interact with water, minerals are formed that are highly reactive with CO_2. These processes naturally occur both at the Earth's surface, where they serve to sequester CO_2 from the atmosphere, and deep in subduction zones, where they play a fundamental role to how crust is recycled and to the generation of earthquakes. Typically, determining the extent to which a rock can trap CO_2 requires extensive sample characterization , which is time- and cost-intensive. The hydration of mantle rocks also result in systematic changes to their physical properties, such as density and reaction to magnetism. These variations in physical properties could be used to identify such rocks using satellite and airborne mapping to rapidly and cheaply identify rocks of interest. We use the chemistry, mineralogy, and physical properties of >400

samples to quantify how these vary during the hydration and carbonation of mantle rocks to develop scientific models that can be used to identify or infer which rocks are the most prospective for carbon sequestration. As some mineral deposits may host rocks suited for carbon sequestration, these physical property constraints presents a means to quantify the potential for a mine to contribute to offsetting CO_2 emissions.

1 Introduction

Ultramafic rocks comprise the largest volumetric portion of the oceanic lithosphere and their alteration is a fundamentally important geologic process on Earth. The high fluid-flow associated with serpentinization alters the physio-chemical properties of the oceanic lithosphere, by weakening and allowing it to flex and subducted more easily, and so contribute to delivering volatiles into the mantle and into the mantle wedge and magmatic arcs (e.g., Escartin et al., 1997; 2001; Guillot and Hattori, 2013). Long-term preservation of ultramafic rocks originating in the oceanic lithosphere (abyssal peridotites) occurs in the geologic record as the lowermost structural portion of ophiolitic sequences that have been obducted during orogeny (Juteau, 2003; Bodinier and Godard, 2014). Ophiolitic ultramafic rocks and their hydrated (serpentinites) and carbonated equivalents are observed in all major Phanerozoic orogenic belts (Bodinier and Godard, 2014 and references therein) and may host Ni-Fe-Cu-PGE mineralization and, thus, have historically been, and continue to be common targets for resource exploration (e.g., Hulbert, 1997; Britton, 2017). Recent work has demonstrated that (serpentinized) ultramafic rocks are particularly reactive with carbon dioxide to the extent that they are prime targets for carbon sequestration (e.g., Kelemen and Matter, 2009; Power et al., 2013; Mervine et al., 2018; Snæbjörnsdóttir et al., 2020; Kelemen et al., 2018; 2020). Mineral carbonation may be achieved using either *ex-situ* or *in-situ* techniques; the former involves exposure of fine-grained material, such as mine tailings, to either atmospheric CO_2 or from a concentrated source, whereas the latter involves injecting CO_2 to a depth of >2 km. *Ex-situ* techniques take advantage of the increased reactive surface area of tailings and the high reactivity of minerals such as brucite (e.g., Power et al., 2013; 2018; 2020; Vanderzee et al., 2019;), whereas *in-situ* techniques exploit the elevated temperatures and pressures at depth to accelerate reactions and fully-carbonate the rock (e.g., Kelemen and Matter, 2009; Kelemen et al., 2018). As resource extraction invariably requires the consumption of energy and emission of CO_2, whether it be for transportation of materials and personnel or for ore processing/extraction, any deposit hosted in ultramafic rocks should explore their potential to sequester CO_2 and so offset or prevent emissions and promote an environmentally sustainable mining industry (e.g., Wilson et al., 2014; Power et al., 2013; 2018; 2020; Hamilton et al., 2020).

Although there are many possible reactions involved in serpentinization (e.g., Toft et al., 1990), the general reaction can be written:

R1: olivine ± orthopyroxene + H_2O => serpentine ± brucite ± magnetite ± alloys/sulphides

Clinopyroxene may also be present; however, it is particularly resistant to alteration and will, instead, typically result in the formation of chlorite or tremolite (Bodinier and Godard, 2014). The abundance of minerals occurring in serpentinites, their chemistry, and the extent of serpentinization are subject to significant variability depending on such factors as olivine/pyroxene in the protolith, extent of melt extraction, Mg/Fe in the primary silicates, pH, silica activity, and oxygen fugacity of the system (e.g., O'Hanley and Dyer, 1993; Evans, 2008; Evans et al., 2009; Klein et al., 2013; Miyoshi et al., 2014; Huang et al., 2017; McCollum et al., 2020a, b; Klein et al., 2020; Peters et al., 2020). Commonly, serpentinization is considered to be largely isochemical with respect to the major element cations (Mg, Fe, Ca, Si), involving primarily the addition of water and the production of hydrogen (e.g., Peters et al., 2020; Niu, 2004; Kodlanyi et al., 2012; Deschamps et al., 2013; Klein et al., 202). However, non-isochemical Si-metasomatism and/or Mg-loss has been inferred to occur in abyssal peridotites at mid-ocean ridges (e.g., Snow and Dick, 1995; Back et al., 2004; Paulick et al., 2006; Malvoisin, 2015).

Highly-serpentinized ultramafic rocks are particularly susceptible to carbonation by CO_2-bearing fluids and follow three general reactions (e.g., Hansen et al., 2005):

R2: olivine + brucite + CO_2 + H_2O => serpentine + magnesite + H_2O

R3: serpentine + CO_2 => magnesite + talc + H_2O

R4: talc + CO_2 => magnesite + quartz + H_2O

Carbonation is also commonly considered to behave isochemically with respect to the major element cations, resulting primarily in the formation of (hydro-)magnesite (e.g., Hansen et al., 2005), except for at high degrees of alteration in which some Ca may be added to the system (e.g., Bideau et al., 1991). These

carbonation reactions serve as a proxy for the reactions that are commonly used in experimental carbon sequestration models (e.g., Power et al., 2020).

Serpentinization and carbonation reactions result in changes in the physical properties of ultramafic rocks, particularly density and magnetic susceptibility (e.g., Toft et al., 1990; Oufi et al., 2002; Maffione et al., 2014; Li et al., 2020); density is directly related to the volume-integrated density of the rock's mineralogy, whereas magnetic susceptibility is related to the concentration, distribution, and size of ferromagnetic minerals—primarily magnetite (Tauxe, 2010; Enkin et al., 2020). Pristine ophiolitic ultramafic rocks should have density and magnetic susceptibility values similar to those of olivine and pyroxene (3.10-3.30 g/cm^3 and ~1 × 10^{-3} SI, respectively). Because serpentinites are dominated by serpentine, brucite (densities of 2.57 and 2.39 g/cm^3, respectively) (O'Hanley, 1996), and magnetite, highly-serpentinized rocks are typically less dense and show a higher magnetic susceptibility than their unaltered protoliths (e.g., Henkel, 1976, Toft et al., 1990; Miller and Christensen, 1997; Maffione et al., 2014; Bonnemains et al., 2016; Li et al., 2020). Serpentinization may also result in a volume increase of up to 40-50% (e.g., Hostetler et al., 1966), although typically serpentinites do not show the particularly high porosity (e.g., Plümper et al., 2012) that would be expected considering such the significant volume change. Carbonation reactions consume serpentine, brucite, and magnetite to form magnesite with subordinate talc and quartz (Kelemen and Matter, 2009; Menzel et al., 2018); magnesite has a density of ~3.00 g/cm^3. Thus, fully carbonated ultramafic rocks should be denser and show lower magnetic susceptibilities than serpentinites (e.g., Hansen et al., 2005).

The physical properties associated with the serpentinization and carbonation of ultramafic rocks have been studied for decades in various capacities (e.g., Burch, 1968; Saad, 1969; Whiteford and Lumb, 1975; Toft et al., 1990; Maffione et al., 2014; Li et al., 2020). However, most studies have focussed on one or the other process (c.f., Toft et al., 1990; Hansen et al., 2005) and typically focus on the behaviour of the volumetrically dominant harzburgitic rocks (e.g., Toft et al., 1990; Maffione et al., 2014). Additionally, most studies focus on either the geochemistry or physical properties of serpentinites. In this contribution, we use >400 samples of variably serpentinized and carbonated ophiolitic ultramafic rocks collected from the Cache Creek/Atlin terrane in the western Canadian Cordillera (Fig. 1) and combine petrographic observations, major element chemistry, quantitative X-ray diffraction analysis (qXRD), and physical properties (magnetic susceptibility, density, porosity, natural remanent magnetization) to constrain the relationships and changes in physical properties that occur during alteration and to determine if and how these may vary as a function of location, protolith, and degree of alteration. Using these results, we present several formulations for determining the %serpentinization of a given sample using chemistry and physical properties and we present a model that uses the physical properties to estimate—at a first order—

the mineralogical variability in ophiolitic ultramafic rocks. Due to the carbonation potential of highly-serpentinized rocks, we use our results to discuss the application of our results to informing geophysical survey analysis with the goal of remotely identifying the most prospective ultramafic rocks for carbon sequestration.

1.1 Study Sites

The 441 samples in this study were collected from the western Canadian Cordillera by various research groups (e.g., Hansen et al., 2004; 2005; McGoldrick et al., 2017; 2018; Milidragovic et al., 2018; Milidragovic and Grundy, 2019; Steinthorsdottir et al., 2020; Zagorevski et al., *in press* and references therein) and these were collected from the traditional territories of the Taku River Klingit, Kaska Dena, Tāłtān Konelīne, Carcross/Tagish, Teslin Tlingit, Tl'azt'en, Binche Whut'en, Yekooche, and Takla First Nations. All localities comprise rocks that are part of the Atlin (equivalent to the undivided Cache Creek in southern B.C.) terrane (Fig. 1), which represents Middle Permian to Middle Triassic discontinuous, dismembered ophiolitic massifs that may have formed either as ocean core complexes or in supra-subduction zone settings (Zagorevksi et al., *in press*). The northern segment is subdivided into the ophiolitic Atlin terrane and sedimentary overlap assemblages of the Cache Creek complex, whereas the southern segment remains undivided (Zagorevski et al., *in press*). The sample set is dominated by rocks from the Decar, Atlin, and Nahlin areas with complementary samples from King Mountain, Hogem, and South Yukon (Table 1). A summary of the sample suites and datasets used as part of this study are provided in Supplementary Table S1 and all sample location information and data are given in Supplementary Table S2.

2 Materials and Methods

We mostly relied on published major element chemistry datasets (Hansen, 2005, McGoldrick et al., 2017; 2018; Milidragovic and Grundy, 2019; Steinthorsdottir, 2021; Zagorevski, 2020). Samples from the Hogem area did not have corresponding published major-element chemistry and these were sent to Geoscience Laboratories for lithogeochemical analysis using the XRF-M01 and IRC-100 packages. Samples that did not have published CO_2 estimates were analysed for their total inorganic carbon (TIC) at the Department of Earch, Ocean and Atmospheric Sciences, University of British Columbia (EOAS-UBC) using a UIC Inc. CM5130 acidification module and a CM5014 carbon dioxide coulometer.

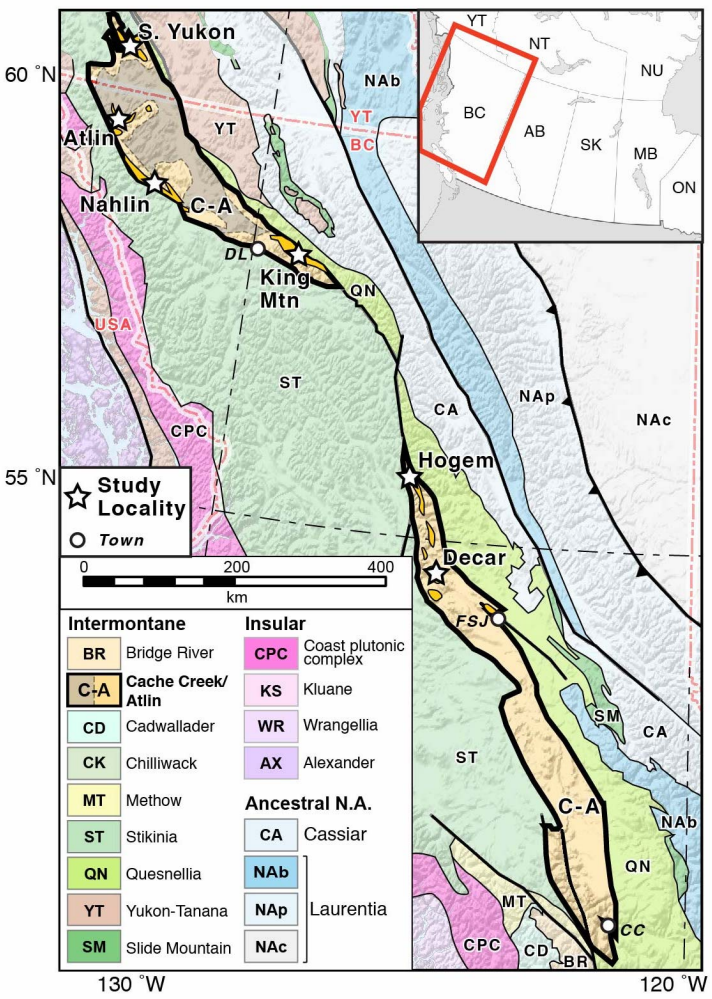

Figure 1. Lithotectonic map of the Canadian Cordillera (after Colpron and Nelson (2011) indicating the six main localities used in this study. Note that the extent of the Cache Creek (grey transparent field) and Atlin terranes are clearly demarcated in northern BC/southern Yukon, whereas they are not sub-divided in the south; subdivision after Zagorevski et al. (2020). Town abbreviations: CC = Cache Creek; DL = Dease Lake; FSJ = Fort St. James. Province abbreviations: BC = British Columbia, AB = Alberta, SK = Saskatchewan, MB = Manitoba, ON = Ontario, YT = Yukon Territory, NT = Northwest Territories, NU = Nunavut.

Quantitative mineralogy for all whole-rock powders was determined by X-ray diffraction at the Electron Microbeam and X-ray Diffraction Facility, EOAS-UBC; Atlin samples of Hansen (2005) were analysed in 2004, whereas all other samples were analysed in 2019-2020; for all instrumentation details and running conditions, see Supplementary Table S3. Qualitative results for Atlin samples are reported in Hansen (2005) and quantitative estimates for the samples were then determined as part of this study. As qXRD estimates for minerals occurring in low abundance (~1 %) are relatively uncertain, brucite

abundances in Decar samples were further characterized by thermogravimetric analysis (TGA) and reported in Steinthorsdottir (2021). The correlation between the two datasets was used to correct the qXRD results, for which there are a greater abundance of data across the sample-set (Supplementary Figure S1). All weight% (wt%) qXRD results have been converted to volume% (vol%) abundances using typical densities for each mineral as this more directly relates to the physical properties.

The magnetic susceptibility and density of all samples were first measured at EOAS-UBC. Magnetic susceptibility (κ) was measured using a ZH Instruments SM30 and applying thickness and demagnetization corrections (Supplementary Table S4 and Supplementary Figure S2). The reported values reflect the mean of five measurements and the uncertainty reflects the 2 SD. Densities were determined using the masses of samples in air and in water using specific gravity mode of an A&D Company Ltd. EJ-6100 balance. To assess the accuracy of our magnetic susceptibility and density measurements, and to provide additional information on the porosity and natural remanent magnetization (NRM), a sub-set of samples that reflect the full diversity of rock types and degrees of alteration were sent to the Paleomagnetism and Petrophysics Laboratory (PPL) at the Geological Survey of Canada–Pacific (GSC-P) in Sidney, British Columbia; all reported porosity and NRM values reflect analyses done the PPL. Measurements at PPL were done on a 2.5 cm diameter core of unweathered material using the methodology and instrumentation as described in Enkin et al. (2020). Comparison of physical property results from EOAS-UBC and GSC-P show a near 1:1 linear relationship with an R^2 of 0.92 for density (Supplementary Figure S3a) and a near-linear relationship of log (magnetic susceptibility) with an R^2 of 0.97. Both datasets show slight offset to higher values for the GSC data (Supplementary Figure S3b) and, as such, EOAS-UBC measurements were corrected based on the relationships of the two datasets. The final physical property values that are reported reflect GSC-P physical property measurements when available, otherwise, the corrected EOAS-UBC were used.

3 Petrographic observations, protoliths, and volatile behaviour

3.1 Petrographic Observations

Relatively fresh dunitic rocks consist dominantly of 1-6 mm-sized equigranular olivine and primary spinel (Fig. 2a). Serpentine in relatively fresh samples is primarily localized along grain boundaries and fine intra-grain fractures (Fig. 2a). With increasing degrees of serpentinization, olivine grains are cut by serpentine veins of increasing thickness (Fig. 2d) until they are fully replaced by mesh texture (Fig. 2g); serpentine occurring as massive veins and as mesh texture are likely lizardite (e.g., Wicks and Whittaker, 1977; Viti, 2010). Brucite increases in abundance with increasing degrees of serpentinization; in fresher rocks it occurs in close association with relict olivine grains, whereas in highly-serpentinized rocks it

occurs as discrete or aggregate grains intergrown with mesh-serpentine or in veins with magnetite. Magnetite is typically absent in the freshest dunitic rocks.

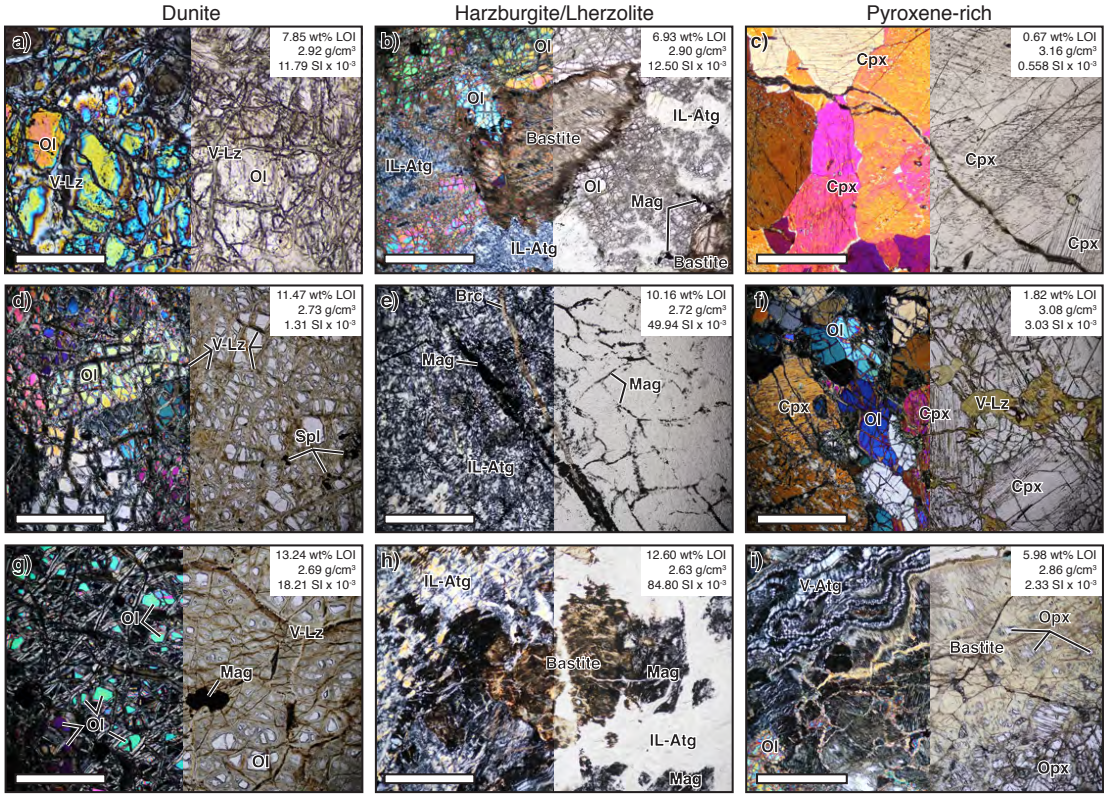

Figure 2. Representative photomicrographs of the main ultramafic protoliths at three increments of their serpentinization process; scale bar in each is 1 mm. Also included for each, are the corresponding LOI (in wt%), density, and magnetic susceptibility. Serpentine in dunite tends to be limited to vein (V-Lz) and mesh-texture lizardite and very little newly formed spinel, whereas serpentine in harzburgite displays interlocking (IL-Atg) and interpenetrating textures typical of antigorite and abundant spinel (magnetite) forms along grain boundaries and as veins. Hydration in pyroxene-rich rocks is focussed on olivine-rich regions and very little spinel is formed.

Fresh harzburgitic/lherzolitic rocks occur in all study areas and consist of anhedral orthopyroxene (2-6 mm-sized) and clinopyroxene (0.5-3 mm-sized), anhedral to euhedral olivine, and subhedral to euhedral equant Cr-spinel (Fig. 2d) (McGoldrick et al., 2018; Milidragovic and Grundy, 2019). Serpentinization in the relatively fresh samples affects olivine almost exclusively, with orthopyroxene, clinopyroxene, and spinel remaining relatively unchanged with the exception of minor magnetite occurring along grain boundaries (Fig 2b, e) and minor orthopyroxene alteration to bastite (McGoldrick et al., 2018). Early serpentinization of olivine in harzburgitic/lherzolitic rocks is similar to dunitic rocks in that it is primarily restricted to cross-cutting lizardite veins (Fig. 2b) that increase in thickness with progressive serpentinization. In the more pervasively serpentinized harzburgitic/lherzolitic rocks, olivine and pyroxene are progressively pseudomorphed by lizardite or antigorite, which occurs as blocky to tabular interlocking crystals in the matrix, as anastomosing vein networks, and as bastite (Fig. 2h). Although the

textures are typical of lizardite and antigorite, the specific serpentine variety was not ascertained. Some pervasively serpentinized samples also exhibit evidence for a third stage of serpentinization involving the formation of chrysotile in veins (e.g., Steinthorsdottir, 2021). Brucite in harzburgitic/lherzolitic rocks that are >60% serpentinized occurs in close association with olivine, as grains in the lizardite groundmass, or as aggregates or veins spatially associated with serpentine and/or magnetite (Fig. 2h). Rocks in which antigorite dominates rarely contain brucite. Magnetite occurs both as a pseudomorph of primary spinel and as newly-formed grains in the serpentine matrix, as veinlets along former grain boundaries, as larger cross-cutting veins and, locally intergrown with awaruite and sulphides (Britten, 2017; Milidragovic and Grundy, 2019); magnetite clearly increases in grain-size and abundance with greater degree of serpentinization (Fig. 2f).

Pyroxene-rich rocks, which include olivine-websterites and websterites/pyroxenites (<10% olivine) are typically relatively fresh (Fig. 2c), with hydration resulting mainly in the replacement of any olivine that is present by serpentine (Fig. 2f, i). As with the other ultramafic protoliths, early serpentinization is localized along olivine intra-grain fractures with progressive serpentinization fully replacing the grains. Brucite is typically not observed in pyroxene-rich lithologies and magnetite occurs in relatively low abundances and is restricted to areas in which olivine has been serpentinized. Pyroxene-rich rocks commonly contain talc, chlorite, and/or tremolite.

Early carbonation consists of thin magnesite-calcite veins cross-cutting serpentine veins, as small grains within a matrix of interlocking antigorite, or within bastite grains. Such rocks are termed ophicarbonates and are characterized by mineral assemblages dominated by serpentine with minor magnesite and talc (<20 vol% each) (Fig. 3a). Progressive carbonation results in the formation of soapstone, which is characterized by a mineralogy dominated by magnesite, with >10 vol% talc, <10 vol% quartz (Fig. 3b), and the gradual disappearance of serpentine from the assemblage. The most highly carbonated rocks are termed listwanite (also referred in the literature to as listvenite, listvanite, or listwaenite) and these consist primarily of magnesite and >10 vol% quartz with minor talc, and local fuchsite (Cr-mica) (Fig. 3c). Brucite in carbonated rocks is restricted to uncarbonated sub-domains in a relatively minor number of ophicarbonates. Magnetite is restricted to relict serpentinite sub-domains in ophicarbonate and soapstone.

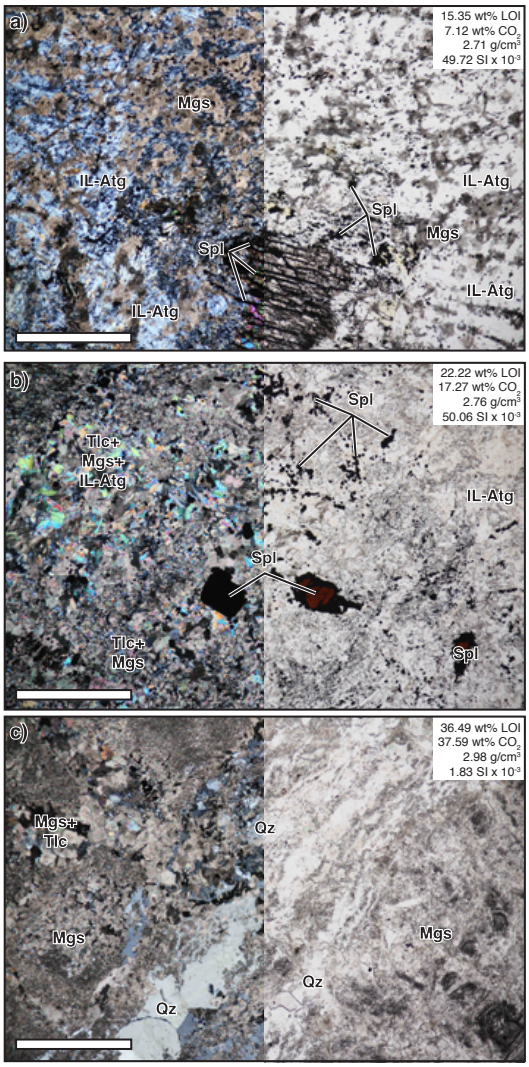

Figure 3. Representative photomicrographs of the three main carbonated assemblages, including the LOI and CO_2 (in wt%), density, and magnetic susceptibility. a) ophicarbonate: abundant serpentine and magnesite with spinel (magnetite) still present in the assemblage; b) soapstone: mainly talc and magnesite with subordinate serpentine and spinel; c) listwanite: dominantly magnesite with sub-domains that include talc or quartz, spinel is rare.

3.2 Protolith discrimination and changes in volatile content

The changes in major element composition during the alteration of ultramafic rocks is generally thought to result from passive dilution by volatiles (e.g., Niu, 2004; Hansen et al., 2005; Deschamps et al., 2013). In such a system, the molar ratio [(Mg+Fe^{tot}+Ca)/Si] (herein referred to as the OPE: olivine-pyroxene-elemental ratio: Steinthorsdottir, 2021) of the samples should provide a reasonable approximation of the olivine/pyroxene in the protolith with OPE >1.93 = opx-poor dunite (95-100 wt% olivine), OPE 1.42-1.93 = opx-rich dunite (90-95 wt% olivine) and harzburgite/lherzolite/wehrlite (50-90 wt% olivine), OPE 1.15-1.42 = olivine websterite (10-50 wt% olivine), and OPE <1.15 = websterite/pyroxenite (<10 wt% olivine); opx-rich dunite was combined with harzburgites as there were not many samples in this category. At a given OPE (isolines in Fig. 4a), the samples show a systematic increase in LOI with decreasing major element cation concentrations, which would support the inference that any changes in major-element chemistry are due to passive volatile dilution. Using the OPE as a

protolith discriminant, most samples have OPE between 1.52 and 1.87, which corresponds to harzburgitic/lherzolitic protoliths (Fig. 4a). For uncarbonated samples (<1 wt% CO_2), these geochemical discriminations are consistent with petrological and textural observations and agree well with various normalizations schemes (Suppl Fig. S4). The same approach could not be used for carbonated samples due to the extensive overprinting of primary textures; instead, these are subdivided on the basis of their mineral assemblages as outlined in section 3.1.

Uncarbonated samples are identified here as having <1 wt% CO_2 and have LOI of up to 14.5 wt%, reflecting the progressive incorporation of H_2O during serpentinization (R1: Fig. 4b). For carbonated samples, changes in their volatile composition involve 1) an increase in CO_2 and decrease in H_2O contents along a linear trajectory (R2-R4: Fig. 4b) from ~12 wt% H_2O and <1 wt% CO_2 to 0 wt% H_2O and 28.99 wt% CO_2 (y-intercept) and 2) continued increase in CO_2 at 0 wt% H_2O. A regression of samples representing R2 to R4 yields a slope of -2.43 ± 0.07 (R^2 = 0.92; n=121: Fig. 4b), which is identical to what would be expected on the basis of changes in the molar mass of a system in which each molecule of H_2O is being replaced by CO_2 (-2.44) (Fig. 4b). Although some samples show small deviations from the expected volatile regression, significant loss or gain of the principal cation constituents would have resulted in deviations from such a trend and more scatter in the regression. This provides additional evidence that the systems appear to have behaved broadly isochemically with respect to the major elements and involved mainly passive dilution due to the addition of volatiles. The continued gain in CO_2 in H_2O-free samples may reflect non-isochemical behavior, mainly in the form of Ca gain (e.g., Bideau et al., 1991).

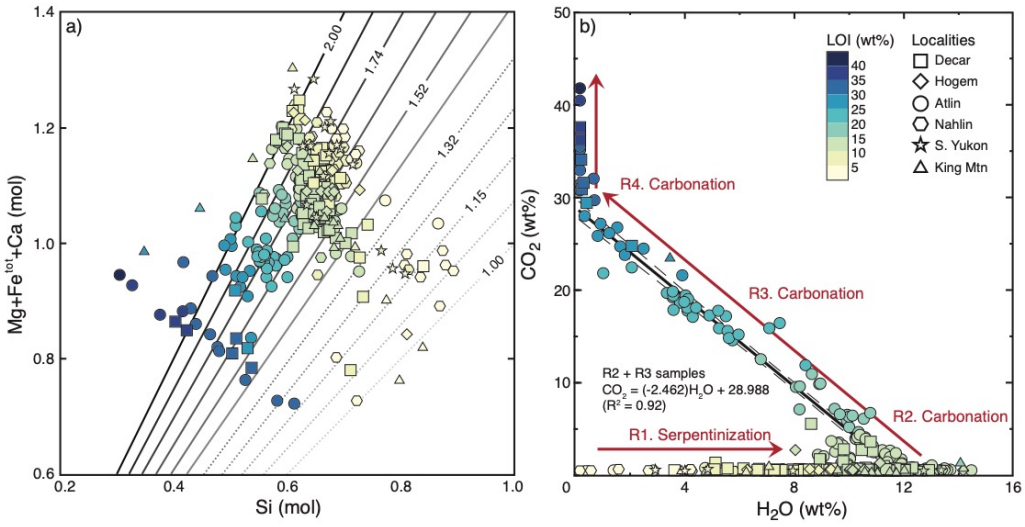

Figure 4. Major element changes with progressive serpentinization and carbonation **a)** Using [(Mg+Fe^{tot}+Ca)/Si] to characterize the proportion of olivine (2.00) to pyroxene (1.00) in the ultramafic protolith; solid isochemical lines indicate a peridotitic protolith, while dashed lines indicate an (olivine-)websteritic protolith. **b)** Serpentinization and carbonation reactions tracked by H_2O and CO_2 contents; concentrations of H_2O are determined by subtracting CO_2 from LOI. Red arrows are the trajectories expected based on changes in the molar proportions of H_2O and CO_2, whereas the solid black line is a regression of samples with CO_2 > 1 wt% and H_2O > 0 wt% and the dashed lines represent the 95% confidence interval (n = 121).

4 Mineralogical and physical property changes during serpentinization and carbonation

4.1 Determining %serpentinization from major-element chemistry

To calibrate LOI as a proxy for degree of serpentinization, the LOI of uncarbonated samples were normalized to their OPE and this was compared to the vol% of non-relict minerals as determined by qXRD (Fig. 5). This normalization accounts for the tendency for olivine-rich samples to yield greater abundances of brucite (e.g., Klein et al., 2020b), which would have a higher bulk-rock LOI at a given %serpentinization due to the greater water content of brucite relative to serpentine (e.g., d'Antonio and Kristensen, 2004). A regression of the data forced through the origin yields a linear relationship for determining %serpentinization:

$$\%serpentinization = 13.3\left(\frac{LOI}{OPE}\right) \quad (eq.\ 1)$$

where LOI is in wt%, OPE is the olivine-pyroxene elemental ratio, and %serpentinization refers to 100% - (vol% olivine+pyroxene). An unforced regression yields a very similar result with a lower intercept that is within error of the origin. We note that qXRD results have typical relative errors of ± 10-15% (Wilson et al., 2009; Turvey et al., 2018) although these effects may be relatively minimal as the data are remarkably consistent despite having been analysed on two different instruments using different analytical procedures and 15 years apart. Additional uncertainty in this formulation may be introduced due to the potential occurrence of primary spinel, secondary metamorphic olivine, or dehydration due to subsequent metamorphism; however, this too we consider to have minimal effect as primary spinel is typical at abundances of <2 vol% and metamorphic olivine is relatively uncommon in the studied samples. From here on, the %serpentinization of any uncarbonated samples use the value determined by *eq.1*.

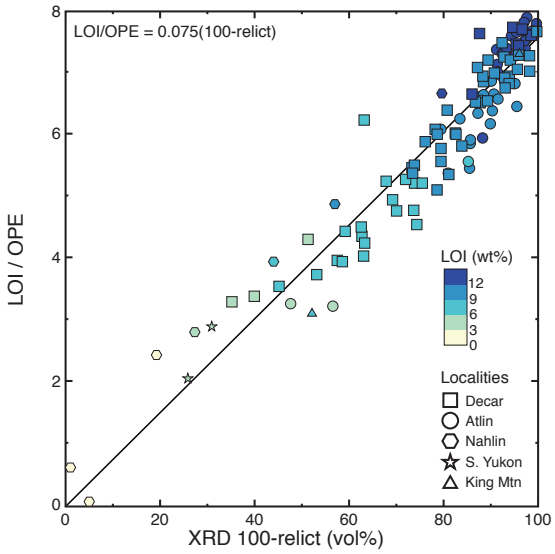

Figure 5. A calibration for determining %serpentinization using loss on ignition (LOI) and olivine-pyroxene elemental (OPE) ratio. The black solid line represents a regression of the sampleset. Note the more condensed colour scale for LOI compared to Figure 4a.

4.2 Changes in mineralogy and physical properties during serpentinization

Weakly-serpentinized (<25 %serpentinized) samples exclusively have OPE <1.42 (Figs. 6, 7) and commonly have CaO contents requiring significant clinopyroxene content; this would dilute the amount of olivine available for serpentinization and is consistent with the higher resistance of clinopyroxene to hydration relative to orthopyroxene and olivine. Moderately to pervasively serpentinized (>25 %serpentinized) samples typically have OPE >1.42 and CaO <1 wt%, indicating that they are dominated by olivine and orthopyroxene. For such rocks, the increasing serpentinization (as indicated by LOI) is also reflected in the quantitative estimates of decreasing relict mineral (olivine+pyroxene) and increasing serpentine abundances (Fig. 6a). Brucite and total spinel (i.e., spinel + magnetite) abundances are variable at a given LOI (0-14 vol% and 0-6 vol%, respectively); however, they occur in rocks with as low as 3-4 wt% LOI (30% serpentinized) and generally increase in abundance with increasing LOI (Fig 6a-inset). Brucite abundances increase for samples with higher OPE (Fig. 7a). Spinel abundances also increase for samples with higher OPE but peak at values of ~1.65 after which abundances decrease; above OPE of 1.93 (>95 vol% olivine) spinel abundances sharply decrease (Fig. 7b). Rocks with very high brucite contents (>6 vol%) typically have low spinel contents (<2 vol%) (Fig. 7).

With increasing serpentinization, the density of the samples decreases consistently from ~3.20 g/cm^3 to ~2.55-2.65 g/cm^3 (Figs. 6b; Fig. 8a, Fig. 9). Within a given interval of low- to moderate-serpentinization (25-50 and 50-75 %), density decreases with increasing OPE; however, above 75

%serpentinization, densities are similar across all samples (Fig. 8). The decreasing density with increasing serpentinization defines a linear relationship (R^2 = 0.94; n=214; 11 rejected) (Fig. 9a):

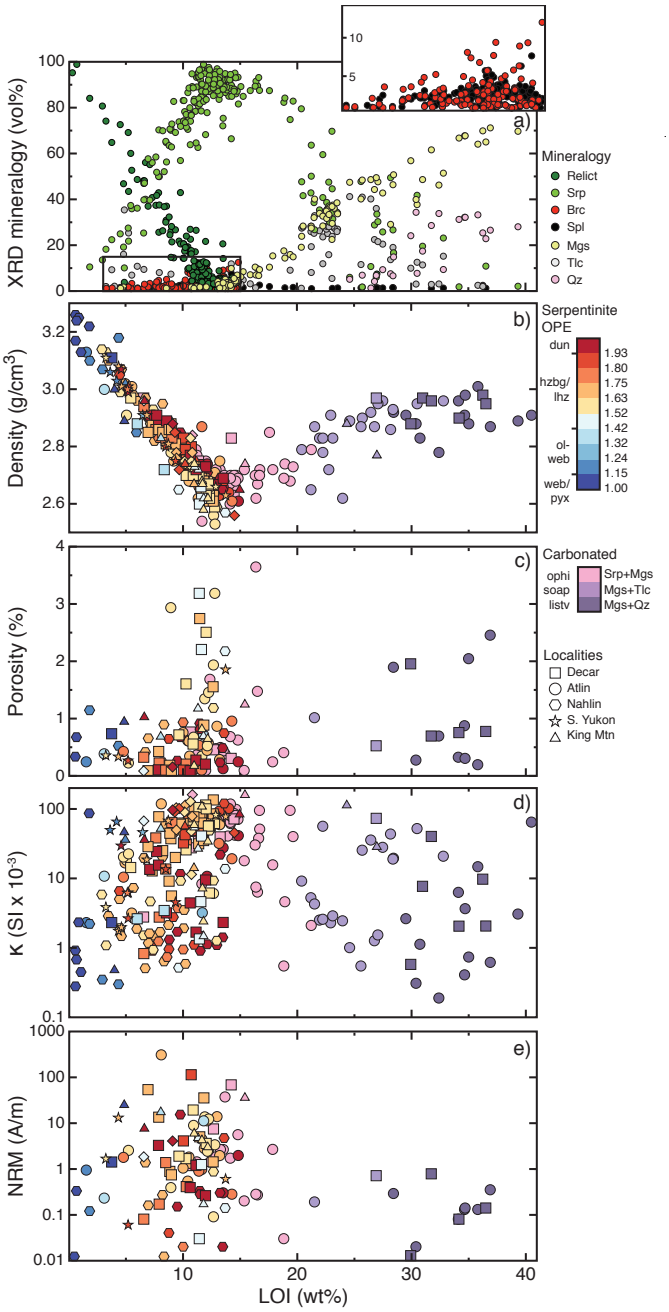

Figure 6. Mineralogical and physical property variations during serpentinization and carbonation; mineral abundances were determined by qXRD and alteration is tracked by changes in volatile content (LOI: wt%). During serpentinization (0-15 wt% LOI) there is a decrease in relict ultramafic mineral and increase in serpentine abundances (a) and this is accompanied by b) consistent decrease in density and a broad increase in c) porosity, d) magnetic susceptibility, and e) natural remanent magnetization (NRM). During carbonation, magnesite abundance increases throughout and talc and quartz occur during intervals of soapstone and listwanite formation, respectively (a). Carbonation is associated with b) increase in density, and decreases in c) porosity, d) magnetic susceptibility, and e) NRM.

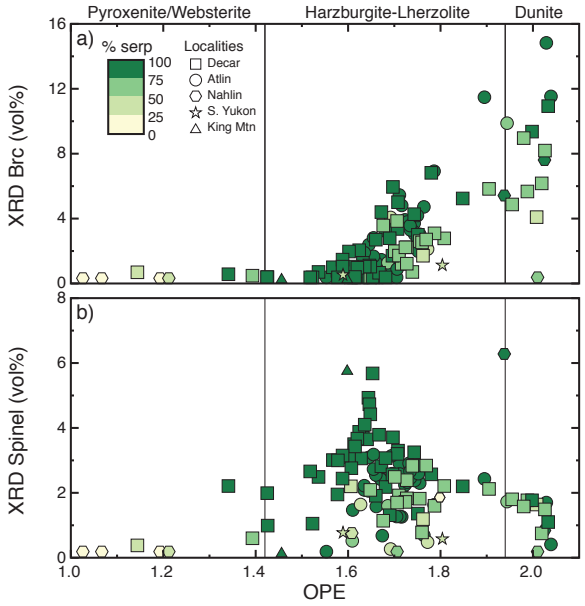

Figure 7. OPE vs. a) brucite and b) total spinel abundance as determined by qXRD. Brucite consistently increases in abundance with increasing OPE and for OPE >1.7 increases with increasing degrees of serpentinization. Spinel abundances are at maximum concentrations for intermediate OPE of 1.65, decrease for both lower and higher OPE, and drop sharply for OPE >1.93.

$$\%serpentinization = -169\ (\pm 3) \times [Density - 3.233(\pm 0.008)] (eq.\ 2)$$

where %serpentinization is defined by *eq. 1*, and density is in g/cm^3; the 11 samples rejected from the regression have residuals outside 2SD of the mean.

Samples typically have porosities of <1 % regardless of the degree of serpentinization and OPE, with the exception of samples with an intermediate OPE of 1.42-1.63 (equivalent to 40-60 vol% olivine) and LOI >10 wt%, which have porosities of up to 3.25 % (Fig. 6c). Density and brucite contents in samples with OPE >1.93 (>95 vol% olivine) show a reasonably systematic correlation ($R^2 = 0.76$) and those with OPE of 1.75-1.93 (70-95 vol% olivine) show a slightly less systematic correlation ($R^2 = 0.42$) (Fig. 9b).

At a given LOI, magnetic susceptibility varies by over two orders of magnitude. Rocks that are <25 %serpentinized have magnetic susceptibilities $<3 \times 10^{-3}$ SI for (Fig. 8). From 25 to 75 % serpentinization, the median values and the range in observed values increases across all OPE classes (Fig 8). Above 75 % serpentinization, samples with OPE between 1.42 and 1.93 (40-95 vol% olivine) show relatively

consistent and high magnetic susceptibilities values, while samples with OPE <1.42 and >1.93 show greater variability and much lower median values (Fig. 8).

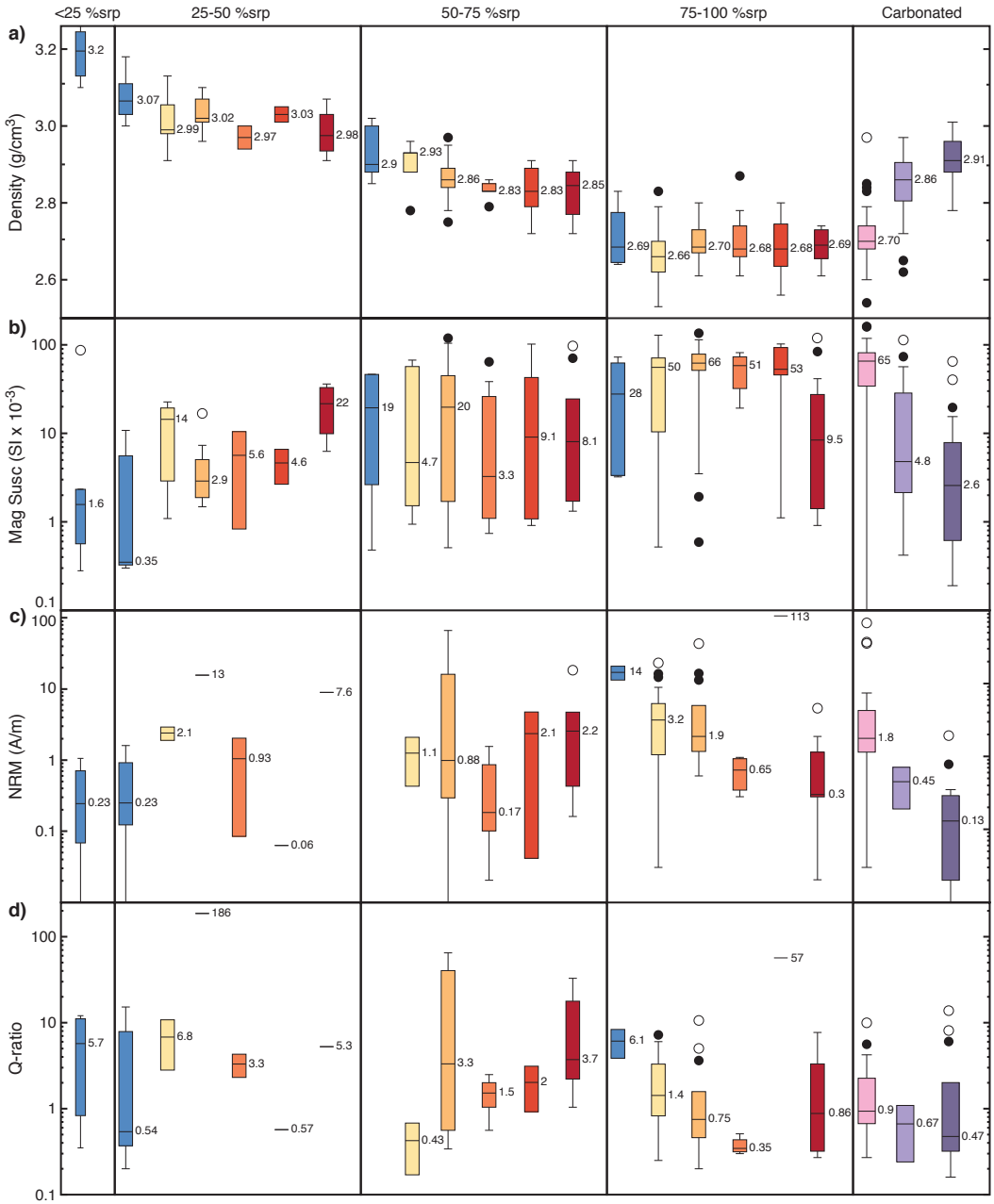

Figure 8. Box-and-whisker plots of density (a), magnetic susceptibility (b), natural remanent magnetization (NRM: c), and Koenigsberger ratio (Q-ratio: d) for various degrees of serpentinization and carbonation. The boxes are drawn around the interquartile range (IQR) with the horizontal line representing the median value; the median is given to the right of its respective box. Whiskers represent minimum and maximum values with outliers excluded, which were determined using the Tukey test where filled circles are beyond 1.5 x IQR and open circles beyond 3 x IQR. Colours for serpentinites reflect the OPE scale shown in Figure 6 with the exception of the blue boxes, which represent all samples with OPE <1.42. Colours for carbonated samples also reflects the symbology shown in Figure 6.

Despite the range in magnetic susceptibilities observed across all lithologies, the general increase in magnetic susceptibility with %serpentinization (Fig. 9c) can be defined by a linear regression anchored at 0 (R^2 = 0.66; n=214; 11 rej):

$$\%serpentinization = \kappa/0.480 \quad (eq.\ 3)$$

where %serpentinization is defined by *eq. 1*, and κ is magnetic susceptibility in SI × 10^{-3}. Although this formulation is by no means robust, magnetic susceptibilities of >20 SI × 10^{-3} rarely occur in samples that are <60 %serpentinized with the exception of those with OPE >1.93. Magnetic susceptibility correlates strongly with spinel contents for the various OPE intervals (R^2 >0.85: Fig. 9d).

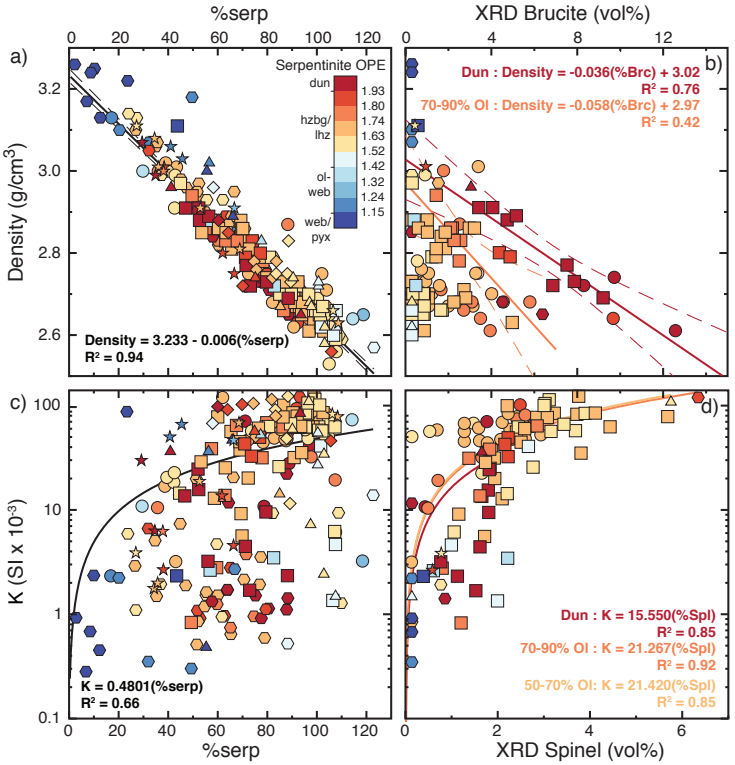

Figure 9. Changes in physical properties as a function of %serpentinization (a and c) and relationships between brucite (b) and spinel (d) abundances and physical properties. a) Density shows an excellent correlation with %serpentinization across all OPE, while c) magnetic susceptibility only shows a reasonable fit (forced through the origin). b) Rocks with OPE >1.93 show an excellent correlation between brucite abundance and density, while those with OPE between 1.74-1.93 show a reasonable correlation; d) Samples with OPE between 1.42-1.93 show a relatively systematic increase in magnetic susceptibility (forced through the origin) as a function of spinel abundance.

The samples show a wide range of natural remanent magnetization (NRM) values, spanning ~4 orders of magnitude and these broadly increase with increasing serpentinization (Fig. 6e; 8c). NRM does

not appear to vary systematically as a function of OPE except for samples that are >75 %serpentinized for which it generally decreases with increasing olivine content. The samples hold relatively high Koenigsberger ratios (Q-ratio) (Fig. 8) with 48% having values greater than 1. Samples that are <50 %serpeninized show a wide range in values that do not vary systematically with increases in %serpentinization or OPE (Fig. 8). For rocks that are 50-75 %serpentinized, samples with OPE >1.42 show increasing Q-ratios with increasing olivine content, whereas rocks that are >75 %serpentinized show the reverse relationship (Fig. 8).

4.3 Changes in mineralogy and physical properties during carbonation

The first phase of carbonation (R2) involves a gradual decrease in serpentine and increase in magnesite abundance, to form ophicarbonate rocks. This is reflected in samples with LOI as low as 8-10 wt% but is most common beginning at ~12-13 wt% LOI; ophicarbonate rocks have LOI up to ~20 wt% (Fig. 6a). The first stage of carbonation is also associated with a disappearance of brucite from the assemblage (Fig. 6a-inset). The physical properties of ophicarbonate samples are indistinguishable from those of highly-serpentinized samples with OPE 1.42-1.93 (Fig. 8).

The second phase of carbonation (R3) is identified by a sharp drop in serpentine abundance concomitant with a more pronounced increase in magnesite and talc abundance to form soapstone (Fig. 6a). The density of soapstone is higher than that of ophicarbonate at ~2.87 g/cm^3 (Fig. 6b; 8a) and porosity is relatively low (<1%: Fig. 6c), while magnetic susceptibility, NRM, and Q-ratio are distinctly lower than serpentinized and ophicarbonate samples (Fig. 6d-e, 8b-d).

The final stage of carbonation (R4) involves the final consumption of serpentine-group minerals, a continued increase in magnesite abundance, a decrease in talc content, and an increase in quartz abundance to form listwanite (Fig. 6a). Such rocks may also locally contain the Cr-mica, fuchsite. The samples show a further increase in density to ~2.91 g/cm^3 (Fig. 6b, 8a), have variable porosity (up to 2.5 %: Fig. 6c), relatively consistent magnetic susceptibility (<10 SI × 10^{-3}: Fig. 6d, 8b), NRM below 1 A/m (Fig. 6e; 8c), and Q-ratios <1 (Fig. 8d).

4.4 Co-variation of density and magnetic susceptibility

On the Henkel plot (density vs. log magnetic susceptibility) the serpentinite samples follow two main trajectories (Fig. 10a). The first involves a linear decrease in density and increase in magnetic susceptibility with serpentinization from ~3.2 g/cm^3 and 0.3 SI × 10^{-3} converging to values of 2.6-2.7 g/cm^3 and 100 SI × 10^{-3}. This defines the trajectory followed by most harzburgitic samples and a very minor proportion of dunitic samples. The second trajectory involves decreasing density with only slight increases in magnetic susceptibility from ~3.2 g/cm^3 and 0.3 SI × 10^{-3} converging to values of 2.6-2.7

g/cm^3 and 0.5-20 SI × 10^{-3}; this is commonly observed for dunitic samples and a relatively minor number of harzburgitic samples. The high susceptibility trajectory is widely reported (e.g., Toft et al., 1990; Maffione et al., 2015; Li et al., 2020); however, the low susceptibility trajectory, although proposed by Toft et al. (1990) on the basis of typical serpentinization reactions; is rarely observed and documented. Toft et al. (1990) proposed that harzburgitic samples would follow the first trajectory regardless of the volumetric proportions of olivine and orthopyroxene (e.g., *eqs 25-32* in Fig. 4D of Toft et al., 1990) and this is clearly reflected in our dataset that show samples with variable OPE converging to a relatively consistent point. The first trajectory also appears to reflect the majority of samples globally (e.g., Toft et al., 1990; Oufi et al., 2002; Maffione et al., 2015; Li et al., 2020). The second low susceptibility trajectory, although not commonly observed or documented, has been proposed to occur for both dunitic and harzburgitic rocks in a high fluid/rock environment (e.g., *Eqs 19-21* in Fig. 4C of Toft et al., 1990).

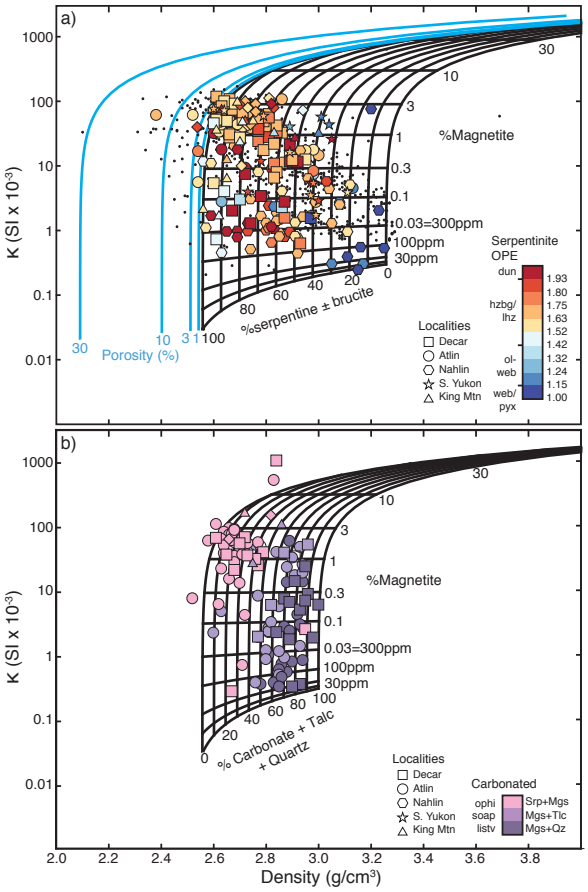

Figure 10. Forward models of ultramafic rock mineralogy shown on the Henkel plot (Density vs. log(magnetic susceptibility) for a) serpentinites and b) carbonated ultramafic rocks. Mineral end-members were estimated based on both the theoretical physical properties and the observed physical properties and quantitative XRD mineral abundances for the samples. Data from Toft et al. (1990) and references therein and Maffione et al. (2014) shown as black data points in part a).

For carbonated rocks (Fig. 10b), the physical properties of ophicarbonate rocks are identical to the majority of highly-serpentinized samples (high magnetic susceptibility and low density). The most prominent change occurs with subsequent carbonation of ophicarbonate samples and is reflected in increasing density and decreasing magnetic susceptibility observed in soapstone and listwanite samples; the main difference between soapstone and listwanite samples is in a slight increase in density.

5 Magnetic susceptibility alone is not an accurate predictor of extent of serpentinization

Most prior studies investigating the physical property changes occurring during serpentinization have been focused on rocks with harzburgitic protoliths (e.g., Toft et al., 1990; Maffione et al., 2014) as they volumetrically comprise the bulk of ophiolitic complexes (Bodinier and Godard, 2014). Our data on rocks spanning the full range of ultramafic protoliths have added new insight into the behaviour of rocks during serpentinization and corroborate the previous works on the stability of magnetite.

Due to the mineralogical simplicity of ultramafic rocks, their chemistry and physical properties vary relatively predictably during serpentinization. We have presented three new formulation (*eqs. 1-3*) for determining the %serpentinization of a given ultramafic rock on the basis of whole-rock major element chemistry (LOI and OPE), density, or magnetic susceptibility, which were calibrated using quantitative mineralogical estimates (Fig. 4); the major-element chemistry- and density-based formulations are far more robust than that based on magnetic susceptibility as has been noted previously (e.g., Oufi et al., 2002; Maffione et al., 2014; Li et al., 2020). The principal requirement for using these formulations is that it must be ascertained that a given sample is minimally carbonated (<1 wt% CO_2). In uncarbonated rocks, increased volumes of brucite will tend to result in higher LOI, while in ophicarbonate rocks, carbonation may not always be obvious petrographically as it can be highly-domainal and fine-grained, which could also potentially skew LOI to higher levels. These two factors could account for inconsistencies observed in using LOI in previous studies (e.g., Deschamps et al., 2013). Density-based calibrations have been previously calibrated (e.g, Miller and Christensen, 1997; Oufi et al., 2002) and yield similar results to *eq 2*; ours differs in that the %serpentinization of the rock has been robustly constrained using quantitative mineralogical determinations and whole-rock chemistry on >200 samples. We have also shown here (Fig. 9b) that for olivine-rich protoliths (>70 vol%) and, specifically for dunitic rocks, density should be a relatively accurate predictor of brucite content and that the nature of the protolith in ophiolitic rocks can be accurately ascertained using OPE.

Estimating %serpentinization using magnetic susceptibility is less reliable than density and chemistry as indicated by the regression statistics in *eq. 3* (R^2=0.66) and as shown in Maffione et al. (2014)(R^2=0.68). This inconsistency is likely a product of factors such as the variability in magnetite behaviour during serpentinization and the role of protolith lithology (olivine/pyroxene), mineral chemistry

(Mg/Fe in the primary silicates), and the extent and conditions of serpentinization (pH, temperature, $aSiO_2$, and oxygen fugacity) in controlling its stability and that of the specific serpentine polymorphs and brucite (e.g., O'Hanley and Dyar, 1993; Evans, 2008; Evans et al., 2009; Miyoshi et al., 2014; Huang et al., 2017; Li et al., 2020; McCollum et al., 2020a, b). This is clearly reflected in our data that show at a given %serpentinization, the spinel abundances are highly variable and so too are the resulting magnetic susceptibilities (Fig. 6c; 8b, 9c). A two-stage serpentinization process for harzburgitic rocks is commonly inferred involving: 1) initial replacement of olivine to form Fe-rich lizardite serpentine and brucite; and 2) orthopyroxene breakdown and Si release, which leads to the formation of more magnesian antigorite serpentine and brucite, magnetite, and hydrogen (e.g., Bach et al., 2006; Beard et al., 2009; Frost et al., 2013; Miyoshi et al., 2014). As dunitic rocks lack or contain only minimal orthopyroxene, only the first serpentinization stage would be expected for such lithologies and magnetite production would not be expected. The dataset presented herein demonstrates this well in that highly-serpentinized dunitic rocks typically contain similar spinel contents to their less-serpentinized equivalents (Fig. 9) and consequently show relatively low magnetic susceptibilities (<10 SI x 10^{-3}) compared to harzburgitic-lherzolitic rocks (Fig. 7), which show consistently high values (>50 SI × 10^{-3}: Fig. 8). This would indicate that, while magnetic susceptibility may be able to accurately identify highly-serpentinized harzburgitic rocks, it may not be able to do so for dunitic or pyroxenite-rich lithologies or to distinguish if they any rocks are slightly carbonated (ophicarbonates rocks).

Although harzburgitic-lherzolitic rocks, in general, behave more predictably in terms of their increased magnetite production with serpentinization, there is a subset of samples with OPE between 1.42 and 1.74 that shows high degrees of serpentinization, but very low magnetic susceptibilities (<10 SI × 10^{-3}) (Fig. 6). These are dominated by samples from the Nahlin locality with a minor number of samples from Decar. The Decar samples exhibiting low magnetic susceptibilities are relatively uncommon and are distinct in that they show evidence for a third stage of serpentinization comprising mainly of chrysotile that overprints the more typical pervasive lizardite and/or antigorite serpentinization (e.g., Milidragovic and Grundy, 2019; Steinthorsdottir, 2021). Since rocks nearby do not show evidence for this third serpentinization phase and do contain abundant magnetite, it is most likely that these samples simply reflect localized regions of transient permeability that destabilized magnetite. Interpretation of the Nahlin samples is more problematic due to a lack of access to the samples or detailed textural documentation of serpentinization. Nevertheless, among the 38 harzburgitic-lherzolitic Nahlin samples, only five of these show magnetic susceptibilities >10 SI × 10^{-3} despite being >50 %serpentinized. There is evidence that the melt-depleted rocks of the Nahlin ophiolite were re-fertilized prior to serpentinization to form intergranular base metal sulphides, clinopyroxene, and Cr-spinel (Lawley et al., 2020). Such an event may be the reason that magnetite formation was inhibited. It would, thus, seem that although magnetic

susceptibility in general tends to behave predictably for harzburgitic rocks, which comprise the bulk of ophiolitic ultramafic rocks, there are locality-specific features or events that may inhibit the use of magnetic susceptibility as a proxy for estimating %serpentinization.

6 Identifying ultramafic carbon sinks using physical properties

Mineral carbonation can occur through either *in-situ* or *ex-situ* methods; the former involves injection of pressurized CO_2 at depths of >2 km (e.g., Kelemen and Matter, 2009), whereas the latter would involve introduction of CO_2 into finely-crushed material at the surface or passive exposure to the atmosphere (e.g., Power et al., 2013). For *ex-situ* carbonation, the occurrence of brucite is key due to its high reactivity at surface pressure and temperature conditions, whereas *in-situ* carbonation models invoke the use of olivine as the prime mineral target for carbonation (Kelemen and Matter, 2009). The CO_2 and H_2O contents of the rocks in this study clearly define two linear arrays (Figure 4B) documenting an initial serpentinization (hydration) event followed by a later carbonation event. No samples have volatile contents that plot between these two arrays suggesting that carbonation only occurred where ultramafic rocks were previously highly serpentinized. We suggest several explanations for this observation:

1. Although serpentinization and carbonation reactions are both thermodynamically favoured at low temperatures (Kelemen et al., 2020), there may be major kinetic barriers to the direct carbonation of olivine and pyroxene (olivine + pyroxene → carbonate + quartz), such that carbonation may only proceed after hydration reactions have created layered silicates (serpentine) and hydroxides (brucite). If serpentinization is a prerequisite for the carbonation of ultramafic rocks, then both *ex-situ* and *in-situ* carbon sequestration plans (e.g., Power et al., 2013; Kelemen and Matter, 2009) should consider targeting serpentinized rather than fresh mantle rock.
2. The restriction of carbonation to previously serpentinized rock may reflect the evolution of fluid pathways in these initially dry ultramafic rocks whereby initial serpentinization caused by the infiltration of H_2O-rich fluids along fractures would increase permeability (e.g., Kelemen and Hirth, 2012), resulting in preferred pathways for fluid flow which were later used by CO_2-bearing fluids. In this scenario, the carbonated portions of the ultramafic massifs in this study all experienced a similar two-stage fluid infiltration history with early H_2O-rich fluids followed by later CO_2-bearing fluids, with the latter only infiltrating fully serpentinized fracture zones.
3. Carbonation is driven by the infiltration of H_2O-rich, CO_2-bearing fluids (e.g., Paukert et al., 2012) that drives serpentinization fronts ahead of carbonation fronts as a natural consequence of the relative abundances of the two chemical components and the fluid composition being buffered by carbonation reactions. If this reaction pathway is a natural consequence of the

infiltration of H_2O-rich, CO_2-bearing fluids into peridotite, then direct carbonation of olivine for *in-situ* carbonation may, instead, require the injection of CO_2-rich solutions, a process for which there appears to minimal evidence in the form of natural analogs.

6.1 Modelling ultramafic rock mineralogy

Maximum serpentine and brucite contents occur in samples with 10 - 14 wt% LOI (>75% serpentinized) (Fig. 6a). In the absence of characterizing the mineral abundance and reactivity of samples in great detail, the physical properties of ultramafic rocks should be effective at predicting—at a first order—mineral content and, thus, a rough estimate of the reactivity of a given volume of rocks. Two approaches for implementing this include: 1) taking physical property measurements of hand-samples or drill-core and/or 2) using physical property models to inform geophysical survey inversions. To do so we follow the methods outlined in Enkin et al. (2020), in which the relationship between physical properties and mineral abundances were used as a forward model to calibrate the Henkel plot (Fig. 10) and then to inverse model the mineralogy based on physical properties. In this approach, minerals with similar physical properties and that behave in a similar way are grouped together into mineral end-members and mixing lines with volumetric proportions are calibrated. Three end-members are used to construct two models: one for (uncarbonated) serpentinites and another for carbonated rocks. In both, end-members and mineral mixing lines are constructed by considering both the theoretical published values for various minerals and the vol% abundance of constituent minerals in the samples as constrained by qXRD.

6.1.1 Forward modelling

For the serpentinites (Fig. 10a), the three mineralogical end-members that we consider are: ultramafic silicates (UM), serpentine and brucite (SB), and magnetite (M). For UM, we use a density of 3.233 g/cm^3 and magnetic susceptibility of 0.3 SI × 10^{-3}; the former is based on the intercept of *eq. 2*, while the latter was chosen to encompass all minimally serpentinized samples. For SB, we use a density of 2.558 g/cm^3 and magnetic susceptibility of 0.03 SI × 10^{-3}; the density was determined from using a 100% serpentinized value applied to equation 2 and then assuming 3 vol% magnetite as this would be consistent with the magnetic susceptibility of the samples. The magnetic susceptibility of the SB component was chosen to encapsulate all uncarbonated samples with minimal porosity. A major unknown for ultramafic rocks is the proportion of primary spinel to magnetite; the former is most common in unserpentinized rocks and cannot be distinguished using XRD. Consequently, for the M endmember we use a density and magnetic susceptibility of 5.20 g/cm^3 and 3000 SI × 10^{-3}, respectively, which is based on empirical studies that suggest these values to be representative of magnetite regardless of grain size (Heider et al., 1996; Peters and Dekkers, 2003). On the Henkel plot for carbonated rocks (Fig 10b), the same SB and M end-members are used for serpentinites but UM is replaced with an endmember reflecting

the physical properties of magnesite (MS); although quartz and talc may also be present in carbonated rocks, magnesite is by far the most volumetrically significant. For MS, we use a density of 3.00 g/cm^3 and magnetic susceptibility of 0.3 SI × 10^{-3}; the former is based on the density of magnesite, while the latter was chosen to fully encapsulate all samples.

6.1.2 Inverse modelling

For rocks that plot within the curves defined by the forward modelling, we can invert the model to provide estimated volumetric mineral abundances. Following the same framework as in Enkin et al. (2020), for the serpentinite model we have three relationships with three unknowns:

$$UM + SB + M = 1$$

$$(UM \times d_{UM}) + (SB \times d_{SB}) + (M \times d_M) = d$$

$$(UM \times K_{UM}) + (SB \times K_{SB}) + (M \times K_M) = K$$

where d = density K = magnetic susceptibility, and UM, SB, and M, refer to the volumetric mineral abundances of ultramafic minerals, serpentine+brucite, and magnetite. These are combined as follows:

$$\begin{pmatrix} 1 & 1 & 1 \\ d_{UM} & d_{SB} & d_M \\ K_{UM} & K_{SB} & K \end{pmatrix} \begin{pmatrix} UM \\ SB \\ M \end{pmatrix} = \begin{pmatrix} 1 \\ d \\ K \end{pmatrix}$$

Thus,

$$\begin{pmatrix} UM \\ SB \\ M \end{pmatrix} = \begin{pmatrix} 1 & 1 & 1 \\ d_{UM} & d_{SB} & d_M \\ K_{UM} & K_{SB} & K_M \end{pmatrix}^{-1} \begin{pmatrix} 1 \\ d \\ K \end{pmatrix}$$

where d_x and K_x refer to the values assigned to the end-member mineral compositions as defined in the forward model, d and K refer to the bulk rock measured density and magnetic susceptibility, respectively. A similar relationship can be constructed for carbonated rocks but substituting the properties for UM with those of MS. When the inverse modelling is applied to the measured physical properties of the serpentinites, the results show a near 1:1 correlation (Fig. 11) for the calculated abundances of hydrous (mostly serpentine and brucite; SB) and primary igneous (olivine+pyroxene; UM) minerals and those determined using qXRD. The model magnetite contents are consistently lower than the total spinel as determined by qXRD, which is incapable of separating out the magnetite concentration; this result is to be expected and the model results are considered an accurate estimate of the abundance of magnetite based on there being no (or only negligible quantities) of other highly magnetic minerals present in these rocks (e.g. magnetic sulphides and alloys).

When the inverse model is applied to the carbonated samples, the carbonation minerals (mostly magnesite+talc+quartz) are consistently overestimated for ophicarbonates and underestimated for listwanites and the opposite is true for hydrous minerals (mostly serpentine). This discrepancy can be explained by the model assumptions that the MS end-member is approximated by the physical properties of magnesite. Overestimation of MS in ophicarbonates could be caused by the presence of relict primary ultramafic minerals, which are still present in such rocks at abundances of up to 15 vol%. Overestimation of MS in listwanites likely reflects the presence of quartz in the assemblage at abundances of up to 20 vol%. The correlation between calculated and qXRD abundances is shown in Fig. 11 and can be used to correct for the systematic bias. In carbonated samples, the calculated magnetite contents of carbonated rocks are highly variable but cluster around the 1:1 line with qXRD spinel abundances. We note that several samples of our samples fall outside the field defined by the mixing lines and would thus yield negative modal abundances according to the inverse model. Samples with densities lower than the SB-M mixing line, likely reflect increased porosity; porosities of 1-4 % are observed in our samples.

6.2 Using geophysics to identify and quantify ultramafic carbon sinks

For a given identified ultramafic body, whose mapped boundaries are relatively well known, the ultimate goal would be to identify and quantify the volumes of serpentinized rocks using remote sensing (i.e. geophysical surveys). The most accurate interpretations of geophysical datasets, such as aeromagnetic or gravity surveys, will involve integration of robust physical property-lithology models. Dunitic protoliths (OPE >1.93) tend to generate the highest brucite content and, thus, will be most reactive, however, harzburgitic rocks (OPE 1.42-1.93) can contain relatively high brucite contents and are volumetrically the most significant in ophiolite massifs and, thus, their physical properties will dominate any geophysical signature.

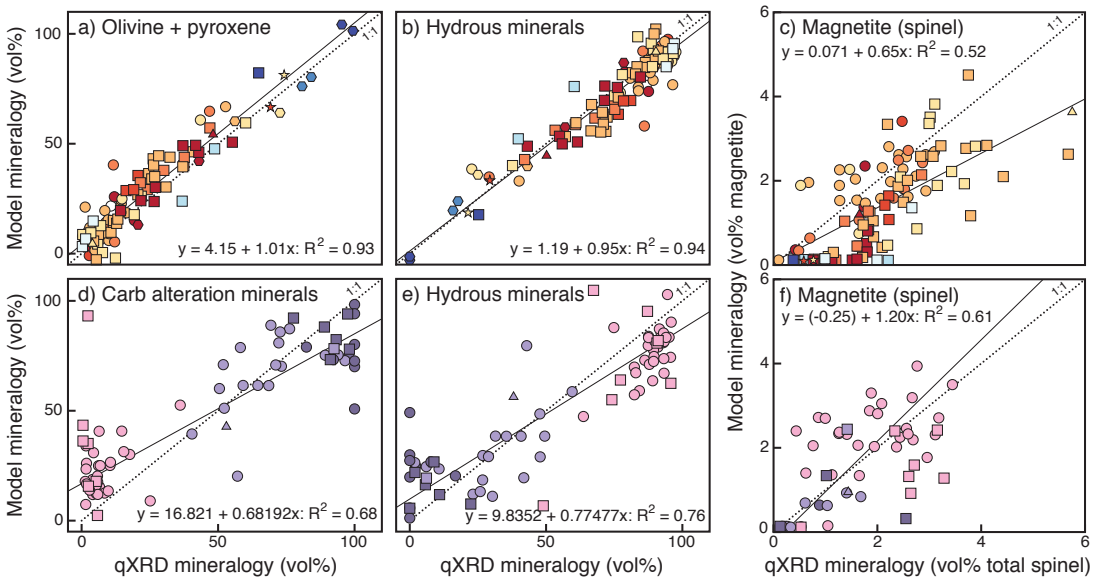

Figure 11. Modelled mineralogy of serpentinites (a-c) and carbonated ultramafic rocks (d-f) compared to mineral abundances as determined by quantitative XRD (qXRD). Hydrous minerals encompasses any minerals formed by the hydration of ultramafic rocks and includes serpentine, brucite, actinolite, and chlorite. Carbonation minerals includes carbonate minerals (magnesite, dolomite, and calcite), talc, and quartz. All regressions (solid lines) were done after omitting outliers, which were identifying by their residuals being outside of 2 SD of the mean.

The systematic drop in density with increased serpentinization across all protoliths indicates that gravity surveys should be the most accurate means for assessing the degree of alteration of a given ultramafic body. If available, and at a sufficiently high resolution, an upper limit of ~2.8 g/cm^3 would be effective at identifying most highly-serpentinized rocks while excluding fresher and moderately- to highly-carbonated rocks. However, high-resolution gravity surveys are expensive. Although using magnetic susceptibility to predict the degree of serpentinization is subject to more unpredictable physical property behaviour, magnetic surveys are more widespread. In general, highly-serpentinized harzburgitic rocks show values of >20 SI × 10^{-3} with median values of >50 SI × 10^{-3}. A lower cut-off of 20 SI × 10^{-3} should identify all highly-serpentinized harzburgitic samples and would exclude many rocks that are <60% serpentinized and those that are moderately- to highly-carbonated (soapstones and listwanites).

We note that weakly-carbonated rocks (ophicarbonates) have identical physical properties to harzburgitic rocks (Figs. 7, 10) and, thus, cannot be discriminated using physical properties and, by extension, geophysical surveys. While the above physical properties limits will result in the identification of false positives—mostly commonly in the form of weakly-carbonated rocks—it will rarely result in false negatives. For *ex-situ* carbonation, which relies on highly-reactive minerals such as brucite that are no longer stable in the presence of any CO_2, the inclusion of ophicarbonates will dilute the overall reactivity of a given volume as ophicarbonate rocks are commonly in close proximity to, or intercalated with, uncarbonated rocks. On the other hand, for *in-situ* carbonation, which could also make use of

serpentine minerals, ophicarbonates are still a viable option given the abundance of such minerals in these rocks.

A complication of applying magnetic susceptibility models to magnetic survey data is that the total magnetization of a given anomaly will reflect a combination of its remanent and induced magnetic fields (Gee and Kent, 2007). Any samples with Koenigsberger ratios (Q-ratio) <1 will have total magnetization signatures dominated by their induced magnetization (magnetic susceptibility). Samples with Q-ratio >1 will have total magnetization signatures dominated by their NRM and the strength of a given anomaly will depend on its coherence (direction). The high Q-ratios recorded in many harzburgitic samples that are <75 %serpentinized (Fig. 8d) likely reflects the lack of high volumes of serpentinization-related magnetite and, thus, relatively low observed magnetic susceptibilities (Fig. 6d; 8a,b). In contrast, the observation of a large range in NRM values (Fig. 6e, Fig. 8a,b) but decreasing median Q-ratios (Fig. 8d) in more serpentinized samples likely reflects the increased magnetite production during serpentinization. In the absence of information on the direction of the preserved NRM, we refrain from calculating hypothetical total effective susceptibilities; future work will include detailed analysis using oriented samples. Nevertheless, the power of physical property models of ultramafic rocks to inform geophysical inversions with the goal of prospecting for serpentinites was demonstrated by Mitchinson et al. (2020). More detailed analysis of NRM will refine such models for a more accurate assessment of the carbon sequestration capacity of a given volume of ultramafic rock.

6.3 Implications for imaging hydration and carbonation in subduction zones

At depths > 30-50 km in subduction zones, H_2O-CO_2 fluids liberated from the downgoing plate infiltrate and react with the overlying forearc mantle wedge, which in turn provides a record of slab-derived fluid infiltration integrated over millions of years (e.g., Hyndman and Peacock, 2003). Experiments by Yardley et al. (2014) demonstrate that hydration reactions are rapid (months to weeks) confirming the rate of serpentinization is likely controlled by the H_2O flux to the reaction front (MacDonald and Fyfe, 1985). The hydration and carbonation history of ultramafic rocks detailed in this study provides insight into similar reactions expected to occur in the mantle wedge. Rock density systematically decreases with increasing serpentinization, but later carbonation increases rock density (Figure 6b) suggesting that gravity data cannot be simply inverted to determine the degree of mantle-wedge serpentinization. Similarly, strong, deep magnetic anomalies have been cited as evidence of extensive forearc serpentinization in Cascadia (Blakely et al., 2005) and other subduction zones. The results presented here suggest serpentinization dramatically increases the magnetic susceptibility of harzburgite, but not dunite. If these results can be extrapolated to the elevated *P-T* conditions of mantle-

wedge serpentinization, this implies that the hydrated Cascadia mantle wedge is made up mostly of harzburgite.

This study documents the sequential replacement of serpentinites during CO_2 infiltration to form magnesite, talc, and ultimately quartz, which occurred, in part because the ultramafic rocks were interleaved with, and obducted onto, carbonate-bearing sedimentary rocks of the Cache Creek terrane (e.g., Zagorevski et al., *in press*). In the case of ultramafic rocks occurring in the mantle wedge in subduction zones worldwide, although the infiltration of CO_2-bearing fluids likely occurs as a result of the subduction of carbonate sediments and carbonate-bearing oceanic crust, the reactions and resulting mineral assemblages would be expected to be similar to those observed here and the resulting rheological changes to subduction zone dynamics could be profound. Specifically, deformation experiments (Escartin et al., 2008; Moore and Lockner, 2008) demonstrate that talc is an extremely weak mineral over a wide range of crustal *P-T* conditions, and serpentinite is dramatically weakened by the presence of minor amounts of talc (Moore and Lockner, 2011). If such minerals were to form along the base of the mantle wedge, this would affect the rheology of the subduction plate interface.

7 Conclusions

We present petrological observations, major-element chemistry, quantitative mineralogy, and physical properties from >400 samples of variably serpentinized and carbonated ophiolitic ultramafic rocks collected from the Cache Creek (Atlin) terrane in British Columbia to constrain the physio-chemical changes that occur during the alteration of ultramafic rocks. The samples show a systematic decrease in density during serpentinization that largely reflects a drop in relict ultramafic mineral abundances and an increase in serpentine minerals and an increase in density during carbonation that mostly reflects the formation of magnesite. The samples show two magnetic susceptibility trends during serpentinization: one involves a 100-fold increase in magnetic susceptibility and is followed by most harzburgitic samples, whereas the second involves very little change in magnetic susceptibility and is followed by most dunitic samples and a minor proportion of harzburgitic samples. Using the quantitative mineralogy and physical property relationships, we provide a model that can be used to estimate the mineralogy of variably-altered ultramafic rocks (at a first-order). These results can be used as a basis for interpreting gravity or magnetic geophysical surveys in order to prospect for the most prospective ultramafic rocks for carbon sequestration and, potentially, to aid in imaging subduction zone lithological heterogeneity.

Acknowledgments, Samples, and Data

All data forming the basis for this paper are available at 10.5281/zenodo.4740942. The authors thank FPX Nickel Corp. and Dejan Milidragovic for facilitating access to samples from the Decar and Hogem areas. Alex Zagorevski is thanked for providing samples and data from the King Mountain, S. Yukon,

Nahlin, and parts of Atlin; these samples were collected as part of the Geo-Mapping for Energy and Minerals-2 (GEM-2) program. The authors also acknowledge that all samples used in this study were collected from the traditional and unceded territories of Taku River Klingit, Kaska Dena, Tāłtān Konelīne, Carcross/Tagish, Teslin Tlingit, Tl'azt'en, Binche Whut'en, Yekooche, and Takla First Nations. Funding is provided by Natural Science and Engineering Research Council (NSERC) discovery grants to GMD (RGPIN-2015-05036) and SMP (RGPIN-2020-07066), and Natural Resources Canada Clean Growth Program grant (CGP-17-0739), and Geoscience BC grant (2018-038) to GMD.

References

Allen, D. E., & Seyfried, W. E. (2003). Compositional controls on vent fluids from ultramafic-hosted hydrothermal systems at midocean ridges: An experimental study at 400 °C, 500 bars. *Geochimica et Cosmochimica Acta, 67,* 1531-1542. https://doi.org/10.1016/S0016-7037(02)01173-0

Ash, C. H. (2001). Relationship between ophiolites and gold-quartz veins in the North American Cordillera. *Ministry of Energy and Mines*, British Columbia Geological Survey Bulletin 108.

Back, W., Garrido, C. J., Paulick, H. Harvey, J., & Rosner, M. (2004). Seawater-peridotite interactions: first insights from ODP Leg 209, MAR 15 N. *Geochemistry, Geophysics, Geosystems, 5(9).* https://doi.org/10.1029/2004GC000744

Bach, W., Paulick, H., Garrido, C.J., Ildefonse, B., Meurer, W.P., & Humphris, S.E. (2006). Unraveling the sequence of serpentinitzation reactions: petrography, mineral chemistry, and petrophyscis of serpentinites from MAR 15ºN (ODP Leg 209, Site 1274). Geophysical Research Letters 33, L13306 https://doi:13310.11029/12006GL025681

Beard, J. S., Frost, B. R., Fryer, P., McCaig, A., Searle, R., Ildefonse, B., Zinin, P., & Sharma, S. K. (2009). Onset and progression of serpentinization and magnetite formation in olivine-rich troctolite from IODP Hole U1309D. *Journal of Petrology, 50*, 387-403. https://doi.org/10.1093/petrology/egp004

Bideau, D., Hebert, R., Hekinian, R., & Cannat, M. (1991). Metamorphism of deep-seated rocks from the Garrett Ultrafast Transform (East Pacific rise near 13º25' S). *Journal of Geophysical Research, Solid Earth 96 (B6),* 10079-10099. https://doi.org/10.1029/91JB00243

Blakely, R.J., Brocher, T.M., and Wells, R.E., (2005) Subduction-zone magnetic anomalies and implications for hydrated forearc mantle. *Geology*, *33*, 445–448. https://doi.org/ 10.1130/G21447.1.

Bodinier, J-L. & Godard, M. (2014) Orogenic, ophiolitic, and abyssal peridotites. *In*: Carlson, R. W. (Eds.*) Treatise of Geochemistry, second edition, 4*, 103-167. https://doi.org/10.1016/B978-0-08-095975-7.00204-7

713 Bonnemains, D., Charlut, J., Escartín, Mével, C., Andreani, M., & Debret, B. (2016). Magnetic signatures
714 of serpentinization at ophiolite complexes. *Geochemistry, Geophysics, Geosystems, 17(8)*,
715 https://doi.org/10.1002/2016GC006321
716 Britten, R. (2017). Regional metallogeny and genesis of a new deposit type—Disseminated awaruite
717 (Ni_3Fe) mineralization hosted in the Cache Creek Terrane. *Economic Geology, 112,* 517-550.
718 https://doi.org/10.2113/econgeo.112.3.517
719 Bursch, S. H. (1968). Tectonic emplacement of the Burro Mountain ultramafic body, southern Santa
720 Lucia Range, California. *Geological Society of America Bulletin 79,* 527-546.
721 https://doi.org/10.1130/0016-7606(1968)79[527:TEOTBM]2.0.CO;2
722 Coleman, R. G. (1977). Part V. Ore deposits in ophiolites. *In:* Ophiolites. Springer-Verlag, Berlin,
723 Germany. Heidelberg press
724 D'Antonio, M, & Kristensen, M. B. (2004). Serpentine and brucite of ultramafic clasts from the South
725 Chamorro Seamount (Ocean Drilling Program Leg 195, Site 1200): inferences for the
726 serpentinization of the Mariana forearc mantle. *Mineralogical Magazine, 68(6)*, 887-904.
727 https://doi.org/10.1180/0026461046860229
728 Deschamps, F., Godard, M., Guillot, S., & Hattori, K. (2013). Geochemistry of subduction zone
729 serpentinites: A review. *Lithos, 178,* 96-127. https://doi.org/10.1016/j.lithos.2013.05.019
730 Dilek, Y. (2003). Ophiolite concept and its evolution. *In:* Dilek, Y. & Newcomb, S. *eds*. Ophiolite
731 concept and the evolution of geological thought. *Geological Society of America- Special Papers*
732 *373,* 1-16. https://doi.org/10.1130/SPE373
733 English, J. M., Mihalynuk, M. G., & Johnston, S. T. (2010). Geochemistry of the northern Cache Creek
734 terrane and implications for accretionary processes in the Canadian Cordillera. *Canadian Journal*
735 *of Earth Sciences, 47,* 13-34. http://https://doi.org/10.1016/j.lithos.2018.06.001
736 Enkin, R. J., Hamilton, T. S. & Morris, W. A. (2020). The Henkel petrophysical plot: mineralogy and
737 lithology from physical properties. *Geochemistry, Geophysics, Geosystems, 20,* e2019GC008818.
738 https://doi.org/10.1029/2019GC008818
739 Escartín, J., Hirth, G., & Evans, B. (1997). Effects of serpentinization on the lithosphere strength and the
740 style of normal faulting at low-spreading ridges. *Earth and Planetary Science Letters, 151,* 181-
741 189. https://doi.org/10.1016/S0012-821X(97)81847-X
742 Escartín, J., Hirth, G., & Evans, B. (2001). Strength of slightly serpentinized peridotites: implications for
743 the tectonics of oceanic lithosphere. *Geology, 29,* 1023-1026. https://doi.org/10.1130/0091-
744 7613(2001)029<1023:SOSSPI>2.0.CO;2

745 Escartin, J., Andreani, M., Hirth, G., & Evans, B. (2008). Relationships between the microstructural
746 evolution and the rheology of talc at elevated pressures and temperatures. *Earth and Planetary*
747 *Science Letters, 268*, 463-475. https://doi.org/10.1016/j.epsl.2008.02.004
748 Evans, B. W. (2008). Control on the products of serpentinization by the Fe^{2+}-Mg_{-1} exchange potential of
749 olivine and orthopyroxene. *Journal of Petrology, 49(10),* 1873-1887.
750 https://doi:10.1093/petrology/egn050
751 Evans, B. W., Kuehner, S. M., & Chopelas, A. (2009). Magnetite-free, yellow lizardite serpentinization of
752 olivine websterite, Canyon Mountain complex, N.E. Oregon. *American Mineralogist, 94*, 1731-
753 1723. https://doi.org/10.2138/am.2009.3301
754 Evans, B. W. (2010). Lizardite versus antigorite serpentinite: magnetite, hydrogen, and life(?). *Geology,*
755 *38,* 879-882. https://doi.org/10.1130/G31158.1
756 Frost, B. R. & Beard, J. S. (2007). On silica activity and serpentinization. *Journal of Petrology, 48(7),*
757 1351-1368. https://doi.org/10.1093/petrology/egm021
758 Frost, B. R., Evans, K. A., Swapp, S. M., Beard, J. S., & Mothersole, F. E. (2013). The process of
759 serpentinization in dunite from New Caledonia. *Lithos, 178,* 24-39.
760 https://doi.org/10.1016/j.lithos.2013.02.002
761 Gee, J. S., and D. V. Kent (2007), 5.12—Source of oceanic magnetic anomalies and the geomagnetic
762 polarity timescale, in Treatise on Geophysics, edited by G. Schubert, pp. 455–507, Elsevier,
763 Amsterdam.
764 Godard, M., Luquot, L., Andreani, M., & Gouze, P. (2013). Incipient hydration of mantle lithosphere at
765 ridges: a reactive-percolation experiment. *Earth and Planetary Science Letters, 371-372,* 92-102.
766 Guillot, S. & Hattori, K. (2013). Serpentinites: essential roles in geodynamics, arc volcanism, sustainable
767 development, and the origin of life. *Elements, 9,* 95-98. https://doi.org/10.2113/gselements.9.2.95
768 Hamilton, J. L., Wilson, S. A., Morgan, B., Harrison, A. L., Turvey, C. C., Paterson, D. J., Dipple, G. M.,
769 & Southam, G. (2020). Accelerating mineral carbonation in ultramafic mine tailings via direct CO2
770 reaction and heap leaching with potential for base metal enrichment and recovery. *Economic*
771 *Geology, 115,* 303-323. https://doi.org/10.5382/econgeo.4710
772 Hansen, L. D. (2005). Geologic setting of listwanite, Atlin, B.C.: implications for carbon dioxide
773 sequestration and lode-gold mineralization. (master's thesis). Retrieved from cIRcle.
774 (https://open.library.ubc.ca/cIRcle/collections/ubctheses/831/items/1.0052391). Vancouver, BC:
775 University of British Columbia.
776 Hansen, L. D., Anderson, R. G., Dipple, G. M., & Nakano, K. (2004). Geological setting of listwanite
777 (carbonated serpentinite) at Atlin, British Columbia: implications for CO2 sequestration and lode-

778 gold mineralization. *Geological Survey of Canada, Current Research 2004-A5*, 12p.
779 https://doi.org/10.4095/216138
780 Hansen, L. D., Dipple, G. M., Gordon, T. M., & Kellett, D. A. (2005). Carbonated serpentinite
781 (listwanite) at Atlin, British Columbia: a geological analogue to carbon sequestration. *The*
782 *Canadian Mineralogist, 43*, 225-239. https://doi.org/10.2113/gscanmin.43.1.225
783 Harrison, A. L., Dipple, G. M., Power, I. M., & Mayer, K. U. (2015). Influence of surface passivation and
784 water content on mineral reactions in unsaturated porous media: implications for brucite
785 carbonation and CO2 sequestration. *Geochimica et Cosmochimica Acta, 148,* 477-495.
786 https://doi.org/10.1016/j.gca.2014.10.020
787 Harvey, J., Savov, I. P., Agostini, S., Cliff, R. A., & Walshaw, R. (2014). Si-metasomatism in
788 serpentinized peridotite: the effects of talc-alteration on strontium and boron isotopes in abyssal
789 serpentinites from Hole 1268a, ODP Leg 209. *Geochimica et Cosmochimica Acta, 126,* 30-48.
790 https://doi.org/10.1016/j.gca.2013.10.035
791 Heider, F., Zitzelsberger, A., & Fabian, K. (1996). Magnetic susceptibility and remanent coercive force in
792 grown magnetite crystals from 0.1 um to 6 mm. *Physics of the Earth and Planetary Interiors*, *93*,
793 239–256.
794 Henkel, H. (1994). Standard diagrams of magnetic properties and density—a tool for understanding
795 magnetic petrology. *Journal of Applied Geophysics, 32(1)*, 43-53. https://doi.org/10.1016/0926-
796 9851(94)90008-6
797 Hostetler, P. B., Coleman, R. G., & Evans, B. W. (1966). Brucite in alpine serpentinites. *American*
798 *Mineralogist, 51, 75*-98
799 Huang, R., Lin, C-T., Sun, W., Zhan, W., & Zhu, J. (2017). The production of iron oxide during peridotite
800 serpentinization: influence of pyroxene. *Geoscience Frontiers, 8,* 1311-1321.
801 https://doi.org/10.1016/j.gsf.2017.01.001
802 Hulbert, L. (1997). Geology and metallogeny of the Kluane mafic-ultramafic belt, Yukon Territory,
803 Canada: eastern Wrangellia—A new Ni-Cu-PGE metallogenic terrane. *Geological Survey of*
804 *Canada, Bulletin 506,* 265p.
805 Hyndman, R.D. & Peacock, S.M. (2003). Serpentinization of the forearc mantle. *Earth and Planetary*
806 *Science Letters, 212,* 417-432.
807 Juteau, T. (2003). Identification of a mantle unit in ophiolites: a major step in the evolution of the
808 ophiolite concept. *In:* Dilek, Y. & Newcomb, S. *eds*. Ophiolite concept and the evolution of
809 geological thought. *Geological Society of America- Special Papers 373,* 1-16.
810 https://doi.org/10.1130/SPE373

811 Katayama, I., Kurosaki, I., & Hirauchi, K. (2010). Low silica activity for hydrogen generation during
812 serpentinization: an example of natural serpentinites in the Mineoka ophiolite complex, central
813 Japan. *Earth and Planetary Science Letters, 298,* 199-204.
814 https://doi.org/10.1016/j.epsl.2010.07.045
815 Kelemen, P. B. & Matter, J. (2009). In situ carbonation of peridotite for CO_2 storage. *Proceedings of the*
816 *National Academy of Sciences, 105(45)*, 17295-17300. https://doi.org/10.1073/pnas.0805794105
817 Kelemen, P.B. & Hirth, G. (2012) Reaction-driven cracking during retrograde metamorphism: Olivine
818 hydration and carbonation. *Earth and Planetary Science Letters, 345-348*, 81-89.
819 https://doi.org/10.1016/j.epsl.2012.06.018
820 Kelemen, P. B., Aines, R., Bennett, E., Benson, S. M., Carter, E., Coggon, J. A., De Obeso, J. C., Evans,
821 O., Gadikota, G., Dipple, G. M., Godard, M., Harris, M., Higgins, J. A., Johnson, K. T. M.,
822 Kourim, F., Lafay, R., Lambart, S., Manning, C. E., Matter, M. M. Michibayashi, K., Morishita, T.,
823 Noël, J., Okazaki, K., Renforth, P., Robinson, B., Savage, H., Skarbek, R., Spiegelman, M. W.,
824 Takazawa, E., Teagle, D., Urai, J. L., & Wilcox, J. (2018). In situ carbon mineralization in
825 ultramafic rocks: natural processes and possible engineered methods. *Energy Procedia, 146,* 92-
826 102. https://doi.org/10.1016/j.egypro.2018.07.013
827 Kelemen, P. B., McQueen, N., Wilcox, J., Renforth, P., Dipple, G., & Vankeuren, A. P. (2020).
828 Engineered carbon mineralization in ultramafic rocks for CO_2 removal from air: review and new
829 insights. *Chemical Geology*
830 Klein, F., Bach, W., & McCollom, T. M. (2013). Compositional controls on hydrogen generation during
831 serpentinization of ultramafic rocks. *Lithos, 178,* 55-69.
832 http://dx.doi.org/10.1016/j.lithos.2013.03.008
833 Klein, F., Humphris, S.E., & Bach, W. (2020). Brucite formation and dissolution in oceanic serpentinite.
834 *Geochemical Perspectives Letters, 16,* 1-5. http://doi: 10.7185/geochemlet.2035
835 Kodolányi, J., Pettke, T., Spandler, C., Kamber, B. S., & Gméling, K. (2012). Geochemistry of ocean
836 floor and fore-arc serpentinites: constraints on the ultramafic input to subduction zones. *Journal of*
837 *Petrology, 53,* 235-270. https://doi.org/10.1093/petrology/egr058
838 Komor, S. C., Elthon, D., & Casey, J. F. (1985). Serpentinization of cumulate ultramafic rocks from the
839 North Arm Mountain massif of the Bay of Islands ophiolite. *Geochimica et Cosmochimica Acta,*
840 *49,* 2331-2338. https://doi.org/10.1016/0016-7037(85)90233-9
841 Lackner, K. S., Butt, D. P., & Wendt, C. H. (1997). Progress on binding CO2 in mineral substrates.
842 *Energy Conversion and Management, 38,* S259-S264. https://doi.org/10.1016/S0196-
843 8904(96)00279-8

844 Lawley, C. J. M., Petts, D. C., Jackson, S. E., Zagorevski, A., Pearson, D. G., Kjarsgaard, B., Savard, D.,
845 & Tschirhart, V. (2020). Precious metal mobility during serpentinization and breakdown of base
846 metal sulphide. *Lithos, 354-355*, 105278. https://doi.org/10.1016/j.lithos.2019.105278
847 Li, Z., Moskowitz, B.M., Zheng, J., Xiong, Q., Zhou, X., Yang, J., Zhang, Y., & Liu, Q. (2020).
848 Petromagnetic characteristics of serpentinization and magnetite formation at the Zedang ophiolite
849 in southern Tibet. *Journal of Geophysical Research: Solid Earth, 125*, e2020JB019696.
850 https://doi.org/10.1029/2020JB019696
851 Macdonald, A. H., & Fyfe, W. S. (1985) Rates of serpentinization in seafloor environments.
852 *Tectonophysics, 116*, 123-135.
853 Maffione, M., Morris, A., Plümper, O., van Hinsbergen, D. J. J. (2014). Magnetic properties of variably
854 serpentinized peridotites and their implications for the evolution of oceanic core complexes.
855 *Geochemistry, Geophysics, Geosystems, 15*. https://doi.org/10.1002/2013GC004993
856 Maher, B. A. (1988. Magnetic properties of some synthetic sub-micron magnetites. *Geophysical Journal*
857 *International, 94,* 83-96. https://doi.org/10.1111/j.1365-246X.1988.tb03429.x
858 Malvoisin, B. (2015). Mass transfer in the oceanic lithosphere: serpentinization is not isochemical. *Earth*
859 *and Planetary Science Letters, 430,* 75-85. http://dx.doi.org/10.1016/j.epsl.2015.07.043
860 McCollum, T.M., Klein, F., Solheid, P., & Moskowitz, B. (2020a). The effect of pH on rates of reaction
861 and hydrogen generation during serpentinization. *Phil. Trans. R. Soc. A*. *378*, 20180428.
862 http://dx.doi.org/10.1098/rsta.2018.0428
863 McCollum, T.M., Klein, F., Moskowitz, B., Berquó, T.S., Bach, W., & Templeton, A.S. (2020b).
864 Hydrogen generation and iron partitioning during experimental serpentinization of an olivine-
865 pyroxene mixture. *Geochimica et Cosmochimica Acta, 282,* 55-75.
866 https://doi.org/10.1016/j.gca.2020.05.016
867 McGoldrick, S., Zagorevski, A., & Canil, D. (2017). Geochemistry of volcanic and plutonic rocks from
868 the Nahlin ophiolite with implications for a Permo-Triassic arc in the Cache Creek terrane,
869 northerwestern British Columbia. *Canadian Journal of Earth Sciences, 54*, 1214-1227.
870 https://doi.org/10.1139/cjes-2017-0069
871 McGoldrick, S., Canil, D., & Zagorevski, A. (2018). Contrasting thermal and melting histories for
872 segments of mantle lithosphere in the Nahlin ophiolite, British Columbia, Canada. *Contributions to*
873 *Mineralogy and Petrology, 173,* 25. https://doi.org/10.1007/s00410-018-1450-9
874 Mervine, E. M., Wison, S. A., Power, I. M., Dipple, G. M., Turvey, C. C., Hamilton, J. L., Vanderzee, S.,
875 Raudsepp, M., Southam, C., Matter, J. M., Kelemen, P. B., Stiefenhofer, J., Miya, Z., & Southam,
876 G. (2018). Potential for offsetting diamond mine carbon emissions through mineral carbonation of

processed kimberlite: an assessment of De Beers mine sites in South Africa and Canada. *Mineralogy and Petrology, 112(2),* 755-765. https://doi.org/10.1007/s00710-018-0589-4

Menzel, M. D., Garrido, C. J., Sánchez-Vizcaíno, V. L., Marchesi, C., Hidas, K., Escayola, M. P., & Huertas, A. D. (2018). Carbonation of mantle peridotite by CO2-rich fluids: the formation of listvenites in the Advocate ophiolite complex (Newfoundland, Canada). *Lithos, 323,* 238-261. https://doi.org/10.1016/j.lithos.2018.06.001

Milidragovic, D. (2019). Geology of the Cache Creek terrane north of Trembleur Lake. *British Columbia Geological Survey Open File 2019-06*, 1:50,000 scale.

Milidragovic, D. & Grundy, R. (2019). Geochemistry and petrology of rocks in the Decar area, central British Columbia: petrologically constrained subdivision of the Cache Creek complex. *In*: Geological Fieldwork 2018, British Columbia Ministry of Energy, Mines and Petroleum Resources, *British Columbia Geological Survey Paper 2019-01*, 55-77.

Milidragovic, D., Grundy, R., & Schiarizza, P. (2018). Geology of the Decar area north of Trembleur Lake, NTS 93K/14. *In*: Geological Fieldwork 2018, British Columbia Ministry of Energy, Mines and Petroleum Resources, *British Columbia Geological Survey Paper 2018-01*, 129-142.

Miller, D. J., & Christensen, N. I. (1997). Seismic velocities of lower crustal and upper mantle rocks from the slow-spreading Mid-Atlantic Ridge, south of the Kane transform zone (MARK). *Proceedings from the Ocean Drilling Program Scientific Results, 153,* 437-454. http://doi:10.2973/odp.proc.sr.153.043.1997

Miyoshi, A., Togiso, T., Ishikawa, N., & Mibe, K. (2014). Role of silica for the progress of serpentinization reactions: constraints from successive changes in the mineralogical textures of serpentinites from Iwanaidake ultramafic body, Japan. *American Mineralogist, 99*, 1035-1044. https://doi.org/10.2138/am.2014.4748

Moore, D. E., & Lockner, D. A. (2008). Talc friction in the temperature range 25°-400°C: Relevance for fault-zone weakening. *Tectonophysics, 449*, 120-132. https://doi.org/10.1016/j.tecto.2007.11.039

Moore, D. E., & Lockner, D. A. (2011). Frictional strengths of talc-serpentine and talc- quartz mixtures. *Journal of Geophysical Research, 116*, B01403. https://doi.org/10.1029/2010JB0 07881

Naldrett, A. J. (2011). Fundamentals of magmatic sulfide deposits. *Economic Geology, 17,* 1-50. https://doi.org/10.5382/Rev.17

Niu, Y. (2004). Bulk-rock major and trace element compositions of abyssal peridotites: implications for mantle melting, melt extraction and post-melting processes beneath mid-ocean ridges. *Journal of Petrology, 45*, 2423-2458. https://doi.org/10.1093/petrology/egh068

O'Hanley, D. S. (1996). Serpentinites, records of tectonic and petrological history. Oxford Monographs on Geology and Geophysics no34.

O'Hanley, D. S. & Dyar, M. D. (1993). The composition of lizardite 1T and the formation of magnetite in serpentinites. *American Mineralogist, 78,* 391-404.

Ootes, L., Bergen, A., Milidragovic, D., & Jones, G.O. (2020). Bedrock geology of the northern Hogem batholith and surroundings, north-central British Columbia. British Columbia Ministry of Mines and Petroleum Resources, *British Columbia Geological Survey Open File 2020-02*, scale 1:50,000.

Oufi, O., Cannat, M., & Horen, H. (2002). Magnetic properties of variably serpentinized abyssal peridotites. *Journal of Geophysical Research, 107(5)*, EPM 3-1EPM 3-10. https://doi:10.1029/2001JB000549

Paukert, A.N., Matter, J.M., Kelemen, P.B., Shock, E.L., & Havig, J.R. (2012). Reaction path modelling of enhanced *in situ* CO2 mineralization for carbon sequestration in the peridotite of the Samail Ophiolite, Sultanate of Oman. *Chemical Geology, 330-331*, 86-100.

Paulick, H., Bach, W., Godard, M., De Hoog, J. C. M., Suhr, G., & Harvey, J. (2006). Geochemistry of abyssal peridotites (mid-Atlantic ridge, 15°20'N, ODP Leg 209); implications for fluid/rock interaction in slow spreading environments. *Chemical Geology, 234(3-4),* 179-210. https://doi.org/10.1016/j.chemgeo.2006.04.011

Peters, C., & Dekkers, M. J. (2003). Selected room temperature magnetic parameters as a function of mineralogy, concentration and grain size. *Physics and Chemistry of the Earth*, *28*, 659–667.

Peters, D., Pettke, T., John, T., & Scambelluri, M. (2020). The role of brucite in water and element cycling during serpentinite subduction – insights from Erro Tobbio (Liguria, Italy). *Lithos, 360-361,* 105431. https://doi.org/10.1016/j.lithos.2020.105431

Plümper, O., Røyne, A., Magraso, A., & Jamtveit, B. (2012). The interface-scale mechanism of reaction-induced fracturing during serpentinization. *Geology, 40*, 1103-1106. https://doi.org/10.1130/G33390.1

Power, I. M., Wilson, S. A., & Dipple, G. M. (2013). Serpentinite carbonation for CO_2 sequestration. *Elements, 9,* 115-121. https://doi:10.2113/gselements.9.2.11

Power, I. M., Harrison, A. L., and Dipple, G. M. (2018). From natural analogues to engineered systems. *Geochemistry of Geologic CO2 Sequestration, 77,* p305. http://dx.doi.org/10.2138/rmg.2013.77.9

Power, I. M., Dipple, G. M., Bradshaw, P. M. D., & Harrison, A. L. (2020). Prospects for CO2 mineralization and enhanced weathering of ultramafic mine tailings from the Baptiste nickel deposit in British Columbia, Canada. *International Journal of Greenhouse Gas Control, 94,* 102895. https://doi.org/10.1016/j.ijggc.2019.102895

Saad, A. H. (1969). Magnetic properties of ultramafic rocks from Red Mountain, California. *Geophysics, 34,* 974-987. https://doi.org/10.1190/1.1440067

Seifritz, W. (1990). CO2 disposal by means of silicates. *Nature, 345,* 486. https://doi.org/10.1038/345486b0

Snæbjörnsdóttir, S. Ó., Sigfússon, B., Marieni, C., Goldberg, D., Gislason, S. R., & Oelkers, E. H. (2020). Carbon dioxide storage through mineral carbonation. *Nature Reviews Earth and Environment, 1,* 90-102. https://doi.org/10.1038/s43017-019-0011-8

Snow, J. E. & Dick, H. J. B. (1995). Pervasive magnesium loss by marine weathering of peridotite. *Geochimica et Cosmochimica Acta, 59(20),* 4219-4235. https://doi.org/10.1016/0016-7037(95)00239-V

Steinthorsdottir, K. (2021). Formation and preservation of brucite and awaruite in a serpentinized ultramafite, central BC: implications for carbon sequestration and nickel recovery. (Master's thesis). Vancouver, BC: The University of British Columbia.

Steinthorsdottir, K., Cutts, J., Dipple., G., Milidragovic, D., & Jones, F. (2020). Origin and serpentinization of ultramafic rocks in dismembered ophiolite north of Trembleur Lake, central British Columbia. *In*: Geological Fieldwork 2019, British Columbia Ministry of Energy, Mines and Petroleum Resources, *British Columbia Geological Survey Paper 2020-01*, 49-58.

Tauxe, L. (2010). *Essentials of Paleomagnetism*, 489 pp., University of California Press, Berkeley.

Thom, J. M., Dipple, G. M., Power, I. M., & Harrison, A. L. (2013). Chrysotile dissolution rates: implications for carbon sequestration. *Applied Geochemistry, 35,* 244-254. https://doi.org/10.1016/j.apgeochem.2013.04.016

Toft, P. B., Arkani-Hamed, J., & Haggerty, S. E. (1990). The effects of serpentinization on density and magnetic susceptibility: a petrophysical model. *Physics of the Earth and Planetary Interiors, 65,* 137-157. https://doi.org/10.1016/0031-9201(90)90082-9

Turvey, C.C., Hamilton, J.L., & Wilson, S.A. (2018). Comparison of Rietveld-compatible structureless fitting analysis for accurate quantification of carbon dioxide fixation in ultramafic mine tailings. *American Mineralogist*, *103(10)*, 1649-1662.

Vanderzee, S.S.S., Dipple, G.M., & Bradshaw, P.M.D. (2019). Targeting highly reactive labile magnesium in ultramafic tailings for greenhouse-gas offsets and potential tailings stabilization at the Baptiste deposit, central British Columbia (NTS 093K/13, 14). *In*: Geoscience BC Summary of Activities 2018: Minerals and Mining, Geoscience BC, Report 2019-1, p. 109-118.

Viti, C. (2010). Serpentine minerals discrimination by thermal analysis. *American Mineralogist, 95(4),* 631-638. https://doi.org/10.2138/am.2010.3366

Whiteford, C. M. & Lumb, J. T. (1975). A catalog of physical properties of rocks, Vol. 3. Listing by Rock type. *Geophysics Division,* N.Z. Geological Survey Department of Scientific and Industrial Research, Willington.

Wicks, F.J., and Whittaker, E.J.W. (1977). Serpentine textures and serpentinization. *The Canadian Mineralogist, 15,* 459-488.

Wilson, S.A., Raudsepp, M., * Dipple, G.M. (2009). Quantifying carbon fixation in trace minerals from processed kimberlite: A comparative study of quantitative methods using x-ray powder diffraction data with applications to Diavik Diamond Mine, Northwest Territories, Canada. *Applied Geochemistry, 24,* 2312-2331.

Wilson, S. A., Harrison, A. L., Dipple, G. M., Power, I. M., Barker, S. L. L., Mayer, K. U., Fallon, S. J., Raudsepp, M. & Southam, G. (2014). Offsetting of CO2 emissions by air capture in mine tailings at the Mount Keith Nickel Mine, Western Australia: Rates, controls and prospects for carbon neutral mining. *International Journal of Greenhouse Gas Control, 25,* 121-140. https://doi.org/10.1016/j.ijggc.2014.04.002

Yardley, B. W. D., Rhede, D., & Heinrich, W. (2014) Rates of retrograde metamorphism and their implications for the rheology of the crust: an experimental study. *Journal of Petrology, 55*, 623-641. https://doi.org/10.1093/petrology/egu001

Zagorevski, A. (2020). Whole-rock geochemical data compilation supporting Geo-mapping for Energy and Minerals Cordillera syntheses, British Columbia and Yukon. *Geological Survey of Canada Open File 8674*, 1 .zip file. https://doi.org/10.4095/323678

Zagorevski, A., Staal, C. R. v., Bédard, J. H., Bogatu, A., Canil, D., Coleman, M., Golding, M., Joyce, N., Lawley, C., McGoldrick, S., Mihalynuk, M., Milidragovic, D., Parsons, A., & Schiarizza, P. (2020). Overview of Cordilleran oceanic terranes and their significance for the tectonic evolution of the northern Cordillera: *Geological Survey of Canada Bulletin 610*.

Geochemistry, Geophysics, Geosystems

Supporting Information for

Deducing mineralogy of serpentinized and carbonated ultramafic rocks using physical properties with implications for carbon sequestration and subduction zone dynamics

J. A. Cutts[1†], K. Steinthorsdottir[1], C. Turvey[1], G. M. Dipple[1], R. J. Enkin[2], and S. M. Peacock[1]

[1]CarbMin Lab, Department of Earth, Ocean and Atmospheric Sciences, The University of British Columbia, Vancouver, BC V6T 1Z4

[2]Geological Survey of Canada-Pacific, Sidney, British Columbia, Canada

Contents of this file

Introduction

Supplementary information for this manuscript comprises six figures (below): S2) Magnetic susceptibility demagnetization corrections; S3) Comparison of density and magnetic susceptibility determined at UBC vs. GSC; and S4) Ultramafic rock classification based on normalized mineralogy abundances. In addition, one Microsoft excel (.xls) file is included that comprises four tabs. Table S1 provides a summary of the samples and number of analyses per locality, Table S2 is the full data compilation, Table S3 shows the instrumentation details and running conditions for qXRD analyses, and Table S4 shows the magnetic susceptibility thickness corrections.

All sample preparation techniques, instrumentation, and analytical conditions are described in the main manuscript and references therein.

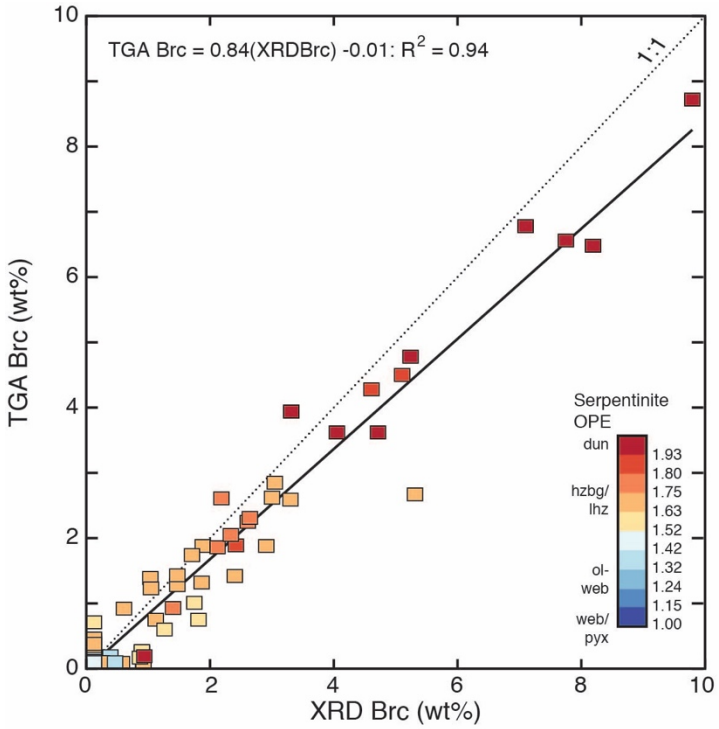

Figure S1. Comparison of brucite abundances determined by quantitative x-ray diffraction and thermogravimetric analysis

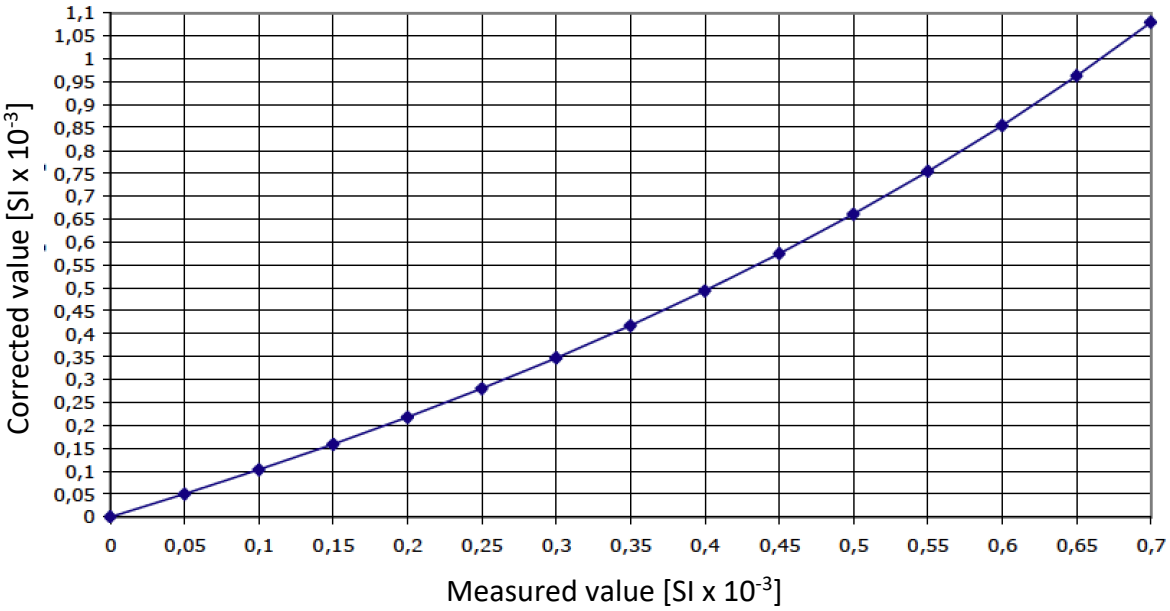

Figure S2. Demagnetization corrections following the instructions manual for the ZH Instruments SM30 magnetic susceptibility meter.

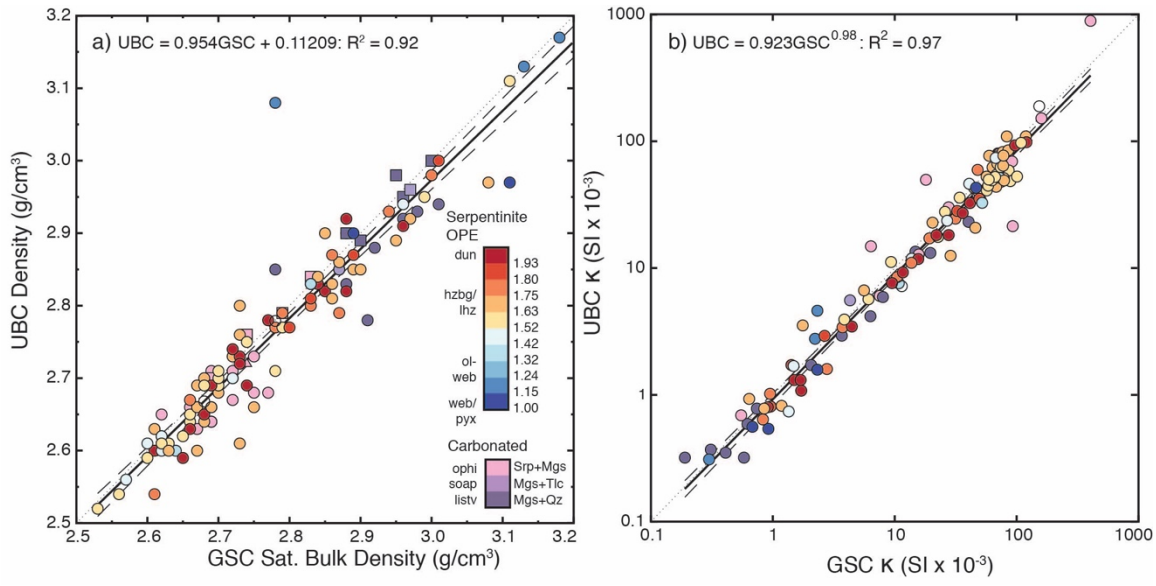

Figure S3. Comparison of a) density and b) magnetic susceptibility measured at UBC and at GSC-PPL

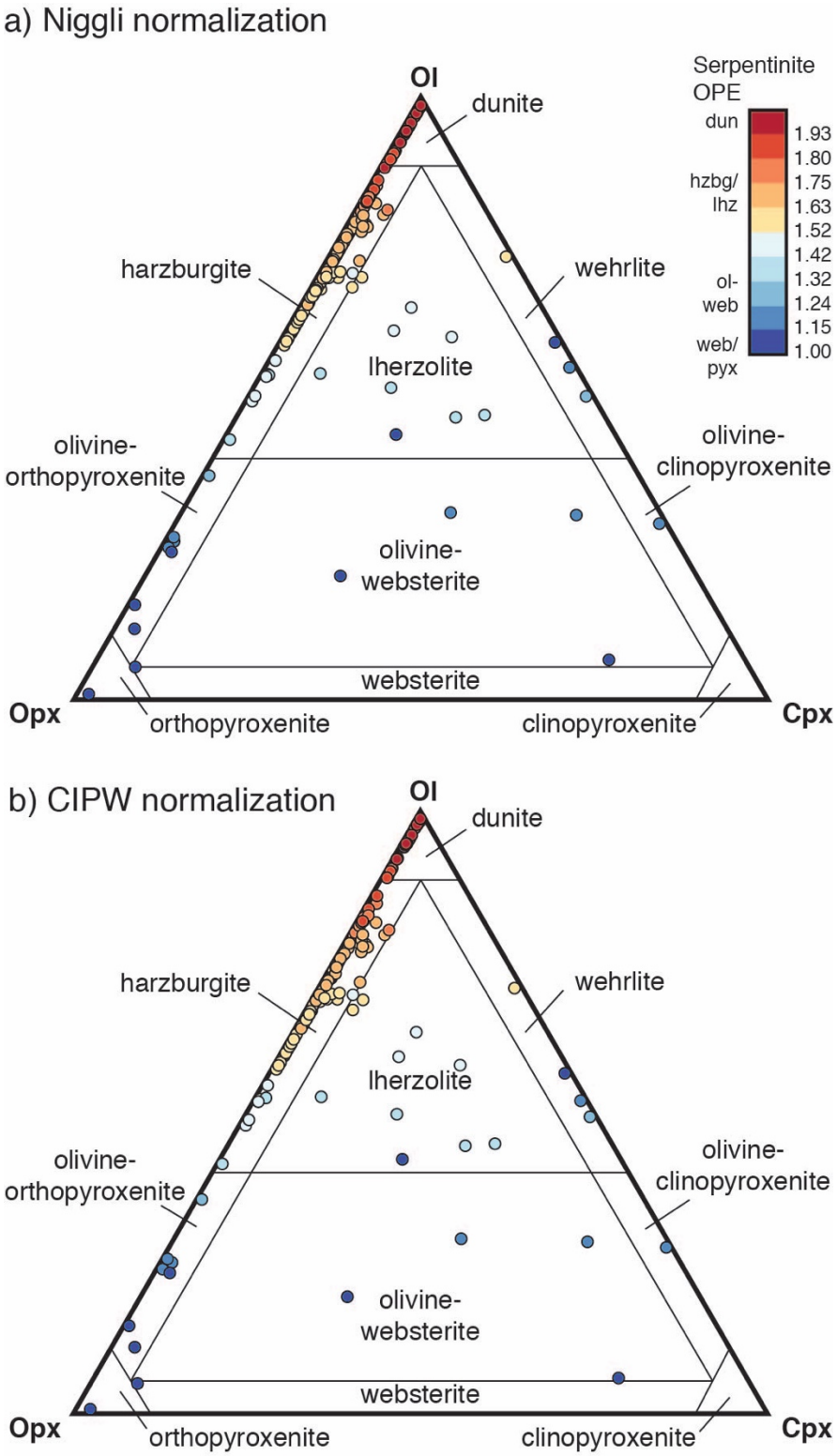

Figure S4. Ultramafic classification ternary diagrams using a) Niggli and b) CIPW normalization mineral abundances. In general, the assigned rock-types on the basis of OPE are similar to those from mineral normalization methods.

Table S1. Summary of the samples and analyses used in this study

Table S2. Compilation of all raw data used in this study.

Table S3. X-ray diffraction instrumentation information, running conditions, and software details

Table S4. Magnetic susceptibility thickness corrections following the instruction manual for the ZH Instruments SM30 magnetic susceptibility meter. Corrections were applied to all magnetic susceptibility measurements done at UBC.